

Reconstructions of the electron dynamics in magnetic field and the geometry of complex Fermi surfaces.

A.Ya. Maltsev

*L.D. Landau Institute for Theoretical Physics of RAS
142432 Chernogolovka, pr. Ak. Semenova 1A, maltsev@itp.ac.ru*

The paper considers the semiclassical dynamics of electrons on complex Fermi surfaces in the presence of strong magnetic fields. The reconstructions of the general topological structure of such dynamics are accompanied by the appearance of closed extremal trajectories of a special form, closely related to geometry and topology of the Fermi surface. The study of oscillation phenomena on such trajectories allows, in particular, to propose a relatively simple method for refining the parameters of the dispersion relation in metals with complex Fermi surfaces.

I. INTRODUCTION

In this paper, we want to consider some issues related to the topological structure of dynamical system

$$\dot{\mathbf{p}} = \frac{e}{c} [\mathbf{v}_{\text{gr}}(\mathbf{p}) \times \mathbf{B}] = \frac{e}{c} [\nabla \epsilon(\mathbf{p}) \times \mathbf{B}] \quad (\text{I.1})$$

that determines the semiclassical dynamics of electrons on the Fermi surface in the presence of an external magnetic field. More precisely, we are interested here in the reconstructions of the topological structure of the system (I.1) that occur when the direction of the magnetic field changes, as well as the relationship between the general picture of such reconstructions and the geometry of the Fermi surface.

Below we explain in more detail what we mean by the reconstruction of the topological structure of the system (I.1), and also give a description of a typical picture of the reconstructions under consideration for rather complex Fermi surfaces. Certainly, we will be most interested in the possibility of experimentally determining the picture of reconstructions of (I.1) on the angular diagram, as well as the possibility of using it to refine the geometry of the Fermi surface (especially in the case of complex surfaces).

As we will see below, both possibilities can actually be associated with the appearance of special extremal (closed) trajectories on the Fermi surface near the boundaries of the reconstructions of (I.1). Moreover, the boundaries of the reconstructions of the structure of system (I.1) can be defined as the boundaries at which trajectories of this type appear and disappear, and the positions of such trajectories on the Fermi surface can be effectively used to refine its geometry. An important role in determining the picture of reconstructions and in restoring the geometry of the Fermi surface will be played by special features of oscillation phenomena, and especially the cyclotron resonance phenomenon on trajectories of this type.

One of the features of the trajectories that we will consider is the presence of (two or more) special points on them at which the electron velocity along the trajectory is very small. This property is due to the proximity of such points to the singular points of the dynamical system (I.1), which, as we have already said, is due to the

connection of the trajectories under consideration with a change in the structure of the dynamical system on the Fermi surface with a change in the direction of \mathbf{B} . The second important feature of the trajectories of interest to us is that they represent “extremal” orbits, i.e. trajectories, the circulation period along which or the area of which have an extremal value in comparison with trajectories close to them. It is not difficult to see that such properties of special trajectories make the study of the associated oscillation phenomena a convenient tool for studying them.

Here, of course, we will not consider in detail the theory of oscillation phenomena in metals (see, for example, [1–3]). We only note here that the main thing for us in the corresponding picture of oscillations having a purely classical (classical cyclotron resonance) or quantum origin (de Haas - Van Alphen effect, Shubnikov - de Haas effect) will be that it is given by the sum of a finite number of oscillation terms (with different periods) corresponding to extremal trajectories on the Fermi surface. The changes in the topological structure of the system (I.1) should correspond then to a sharp change in the general picture of oscillations, consisting in the disappearance of some oscillation terms in the sum and their replacement with new ones. Thus, we expect the observation of sharp changes of the described type on some net of one-dimensional curves (on the angular diagram) corresponding to reconstructions of the topological structure of the system (I.1).

As for the special position of the trajectories under consideration on the Fermi surface, it is in fact due to the proximity of such trajectories to the very special singular trajectories of the dynamical system (I.1). Trajectories of the latter type can arise only for special directions of \mathbf{B} (defined by the picture of reconstructions of (I.1) at the angular diagram) and are associated with exact geometric parameters of the Fermi surface. We will examine the situation in more detail in just a few paragraphs below.

As is well known, the geometry of the trajectories of the system (I.1) plays a crucial role in the theory of galvanomagnetic phenomena in metals in the presence of strong magnetic fields. In particular, as was first shown in [4], the behavior of conductivity in strong magnetic fields

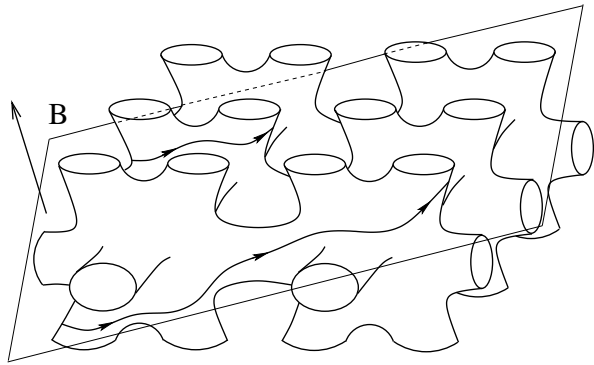


FIG. 1: The intersection of a rather complex periodic surface in the space of quasimomenta by a family of planes orthogonal to the magnetic field.

should differ significantly in cases where only closed trajectories of (I.1) present on the Fermi surface and when open trajectories also appear on it. Further studies of the behavior of the trajectories of the system (I.1) on various Fermi surfaces and effects related to their geometry were carried out very actively, starting from the middle of the last century, in particular, a huge role in the formation and development of this area was played by studies conducted by I.M. Lifshits school during this period (see [2, 5–11]). It should also be noted that studies related to the geometry of trajectories of (I.1) have become the source of a number of approaches and methods for studying electronic spectra in metals, which have not lost their relevance at present.

The problem of a complete description of all types of trajectories of the system (I.1) for an arbitrary periodic relation $\epsilon(\mathbf{p})$ was first set by S.P. Novikov in [12] and intensively studied in his topological school (S.P. Novikov, A.V. Zorich, S.P. Tsarev, I.A. Dynnikov [12–20]). In studying the Novikov problem, in particular, new types of open trajectories ([15, 19]) were found that were previously unknown for the systems (I.1). Note that since the system (I.1) conserves the electron energy $\epsilon(\mathbf{p})$ and the projection of the quasimomentum \mathbf{p} on the direction of the magnetic field, the Novikov problem can also be posed as the problem of describing the geometry of all possible sections of an arbitrary periodic surface by a family of parallel planes in \mathbf{p} -space (Fig. 1). At present, a complete classification of various types of trajectories for arbitrary dispersion relations $\epsilon(\mathbf{p})$ is obtained (see [18–20]), among which the most important are stable open trajectories of (I.1).

For the description of the galvanomagnetic phenomena in strong magnetic fields, the angular diagrams for magnetoconductivity are usually used, which reflect the appearance of various types of trajectories (primarily open) on the Fermi surface for different directions of \mathbf{B} . Since the appearance of various types of trajectories in this

case is directly related to changes in the structure of the system (I.1), such diagrams are, in fact, closely related to angular diagrams reflecting changes in the topological structure of (I.1), which we will consider below. In particular, the appearance of trajectories of the type of interest to us is also associated with the appearance of open trajectories, so that they always arise when the directions of the magnetic field are close to the directions of the appearance of open trajectories on the Fermi surface. The appearance of our trajectories in this case is connected with (infinite) sequences of reconstructions of trajectories of system (I.1) when open trajectories appear. As a result of this, the richest structures at the angular diagrams describing the reconstructions of the topological structure of the system (I.1) are, in fact, associated with open trajectories of (I.1), and such diagrams are in some sense “attached” to the angular diagrams for magnetoconductivity in the case of rather complex Fermi surfaces.

In the most general case, however, the appearance of trajectories of the type of interest to us may not be related to the appearance or disappearance of open trajectories, however, it always corresponds to a reconstruction of the “topological structure” generated by trajectories of (I.1) on the Fermi surface. Moreover, to describe the reconstructions of the topological structure of (I.1) it is enough, in fact, to monitor changes of closed trajectories, which explains the close connection of the trajectories of interest to us with such reconstructions. In a sense, one can say even more, namely, for a sufficiently comprehensive description of the topological structure of the system (I.1) on a two-dimensional periodic surface, in fact, information on the structure of closed trajectories arising on it is sufficient. The formulated statement can be explained as follows. The indication of the complete set \mathcal{M} of closed trajectories of the system (I.1) also uniquely determines its complement on the Fermi surface, consisting of a finite number of (nonequivalent) connected components carrying open trajectories of the system (I.1). As follows from rather deep topological studies (see [13–21]), the main features of the geometry of open trajectories of (I.1) are completely determined by the topology of the components that support them (more precisely, by the genus of the corresponding compact manifolds obtained after factorization by the reciprocal lattice vectors). Thus, the indication of the complete set of nonequivalent closed trajectories of the system (I.1) on the Fermi surface actually determines the complete structure of the system (I.1) on it, that is, allows us to effectively describe all the trajectories arising on it. Below we discuss the statements made in more detail.

All nonsingular closed trajectories of system (I.1) on the Fermi surface are combined into a finite number of (nonequivalent) cylinders of such trajectories having singular points of system (I.1) on their bases (Fig. 2). For structures in general position, we can assume that exactly one singular point presents on each of the bases of the cylinders of closed trajectories of (I.1). A change

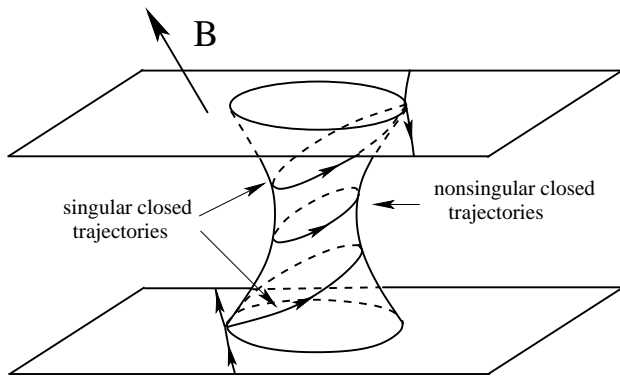


FIG. 2: The cylinder of closed trajectories of system (I.1) on the Fermi surface, bounded by singular trajectories on its bases.

in the structure of the trajectories of the system (I.1) is always associated with a change in the set of cylinders of closed trajectories (for example, with rotations of the direction of \mathbf{B} or a change in the Fermi level), i.e. the disappearance of part (or all) of such cylinders and the appearance of new ones (or the complete disappearance of closed trajectories on the Fermi surface). It is not difficult to see that the disappearance (or appearance) of a cylinder of closed trajectories must be associated with the appearance of special singular trajectories of the system (I.1) (or “cylinders of zero height”) connecting more than one singular point of (I.1).

As we have already said, we are primarily interested here in a change in the structure of the trajectories of the system (I.1) under rotations of the magnetic field direction. According to the above, the entire space of directions of \mathbf{B} (that is, the unit sphere \mathbb{S}^2) can be divided into regions (as well as limit sets of such regions), in each of which the topological structure of system (I.1) on the Fermi surface remains unchanged. The boundaries of these regions are determined by the disappearance (or appearance) of at least one of the cylinders of closed trajectories, i.e. the presence of at least one “cylinder of zero height” at the corresponding directions of \mathbf{B} . It is easy to see that near the boundaries of the reconstructions of the structure of (I.1) we should expect the appearance of cylinders of closed trajectories of very small height, giving in the limit “cylinders of zero height” on the Fermi surface. A special feature of closed trajectories on cylinders of small height is their proximity to singular trajectories and, in particular, to the critical singular trajectory that appears at the moment of reconstruction of the structure of (I.1). As with any cylinder of closed trajectories, on cylinders of small height up to the moment of reconstruction, extremal closed trajectories with the minimal circulation period among all trajectories of the cylinder are preserved. It is precisely such trajectories that we will mainly consider in this paper.

As we will see below, reconstructions of system (I.1) can have different topology, and the corresponding special extremal trajectories can have different geometry. Here we will list the topological types of reconstruction of (I.1) and present the corresponding geometric types of special trajectories. In this paper, we will examine in more detail one of the simplest types, which occurs, in reality, in the vast majority of cases for real Fermi surfaces. As an example of the use of special trajectories, we will give here one of the possible methods for partial restoration of the shape of the Fermi surface using trajectories of this type. In the general case, however, it can be noted that the above method is not the only possible one.

In general, we would like to describe here typical pictures of reconstructions of the structure of system (I.1) on the angular diagram for all directions of \mathbf{B} , discuss the topological types of such reconstructions and the geometry of the corresponding special extremal trajectories, and discuss special features of oscillation phenomena under structural reconstructions of (I.1), as well as the possibility of using information about such reconstructions for the determination of the shape of the Fermi surface.

As an example of describing the complete structure of the system (I.1) in the presence of open trajectories and its relationship to closed trajectories, we give in Chapters 2 and 3 a brief description of the topological structure of system (I.1) on the Fermi surface in the presence of stable open trajectories of this system. In this situation, we will mainly be interested in the procedure of crossing the boundary of the region corresponding to the existence of stable open trajectories of the system (I.1) on the Fermi surface, as well as the structure of closed trajectories near its borders. As we will see, in addition to the above-mentioned features (the existence of sections with a very low trajectory speed), the closed trajectories that appear here may have many additional interesting properties arising from their geometry. Note here that such regions, as is well known, can only occur for Fermi surfaces of sufficiently complex shape (open Fermi surfaces). In Chapter 3, we will also then consider the general structure of diagrams describing reconstructions of the structure of system (I.1) and their relationship to the angular diagrams for magnetic conductivity, and discuss the complexity classes of such diagrams.

In Chapter 4, we will look in more detail at the schemes of “elementary” reconstructions of the structure of system (I.1) and discuss the probability of different types of reconstructions appearing on real Fermi surfaces.

In Chapter 5, we will consider the relationship of the phenomena we are considering with the general geometry of the Fermi surface and, in particular, discuss the possibilities of using the observation of such phenomena to study the features of the electron spectrum.

In Chapter 6, we will discuss some features of oscillation phenomena associated with trajectories of the type we are interested in, where we will consider in particular the observation of the phenomenon of cyclotron reso-

nance on such trajectories.

II. TOPOLOGICAL STRUCTURE OF THE SYSTEM (I.1) IN THE PRESENCE OF STABLE OPEN TRAJECTORIES ON THE FERMI SURFACE

For the purposes of this work, we will need, in particular, a description of topological structure of the system (I.1) in the presence of stable open trajectories on the Fermi surface. Trajectories of this type are stable with respect to small rotations of the direction of \mathbf{B} , and their presence means in fact that the corresponding direction of \mathbf{B} belongs to some “Stability Zone” in the space of directions of \mathbf{B} (i.e. on the unit sphere \mathbb{S}^2).

As we have already said, in description of the topological structure of dynamical system (I.1), the structure of the set of closed trajectories arising on the Fermi surface plays the most important role. Let us illustrate here the relationship of this structure to the complete structure of the system in the presence of stable open trajectories on the Fermi surface.

Using the information about the set \mathcal{M} of cylinders of closed trajectories, we define the following procedure of simplifying (reducing) the Fermi surface (see [20]) for a given direction of the magnetic field:

- 1) Remove all cylinders of closed trajectories from the Fermi surface (Fig. 3). (The rest of the Fermi surface contains only singular and open trajectories of the system (I.1), so its connected components can be called “carriers” of open trajectories).

- 2) Glue the resulting holes with flat disks in the \mathbf{p} -space, orthogonal to \mathbf{B} . The result of the reduction will again be a periodic two-dimensional surface in \mathbf{p} -space, now carrying only open trajectories of system (I.1).

The most important property (see [13, 16]) of a reduced Fermi surface in the presence of stable open trajectories of the system (I.1) is that all its connected components in this case are periodically deformed planes having the same integral direction in \mathbf{p} -space (Fig. 4). Thus, all carriers of open trajectories form a set of parallel periodically deformed planes with a common (two-dimensional) direction generated by two arbitrary reciprocal lattice vectors. The number of nonequivalent such planes is an even number, and for Fermi surfaces of a not very large genus cannot actually exceed two.

In general, the structure of the original Fermi surface carrying stable open trajectories of system (I.1) can be schematically represented by the picture shown at Fig. 5. We can see that this structure remains the same for all rotations of the direction of \mathbf{B} until at least one of the cylinders of closed trajectories connecting the carriers of open trajectories in \mathbf{p} -space is destroyed. The invariance of the topological structure of the system (I.1) on the Fermi surface means, in particular, the invariance of homological cycles defined by the circles that “cut” the Fermi surface into carriers of open trajectories, and the

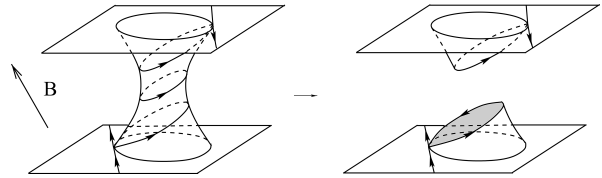


FIG. 3: Removing the cylinder of closed trajectories from the Fermi surface, followed by gluing the holes with disks orthogonal to the magnetic field.

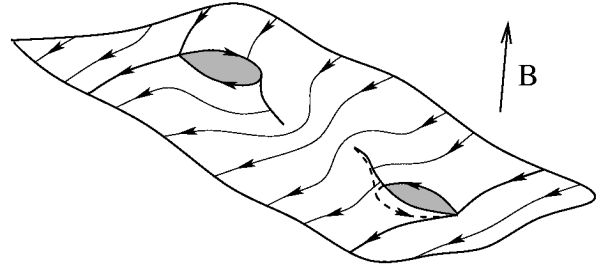


FIG. 4: The connected component of the reduced Fermi surface, carrying stable open trajectories of the system (I.1).

invariance of the topology of the carriers of open trajectories, as well as the topological class of embedding of carriers in the \mathbf{p} -space (more precisely, the homological class of embedding of two-dimensional tori \mathbb{T}^2 , i.e. carriers factorized by the vectors of the reciprocal lattice, into the three-dimensional torus \mathbb{T}^3 , i.e. the compactified Brillouin zone, defined by the integral two-dimensional direction of embedding of carriers in the \mathbf{p} -space). Fig. 5, of course, is only a schematic representation of the topological structure of the system (I.1) on the Fermi surface, and the real picture may look much more complex from a visual point of view. In particular, cylinders of closed trajectories can have a fairly small height and pass through a large number of Brillouin zones for structures with large homological classes of embedding $\mathbb{T}^2 \rightarrow \mathbb{T}^3$.

As can also be seen from Fig. 5, among the cylinders of closed trajectories on the Fermi surface, “simple” cylinders of closed trajectories can occur, one of the bases of which is tightened into a single singular point (Fig. 6).

The appearance and disappearance of cylinders of this type, generally speaking, changes the general topological structure of the system (I.1) on the Fermi surface. Usually, however, the presence or absence of such cylinders does not play a big role in describing the complex geometric properties of trajectories of system (I.1). Here, too, we are mainly interested only in reconstructions of the structure of (I.1) with the disappearance or appearance of “non-trivial” cylinders of closed trajectories (Fig. 2).

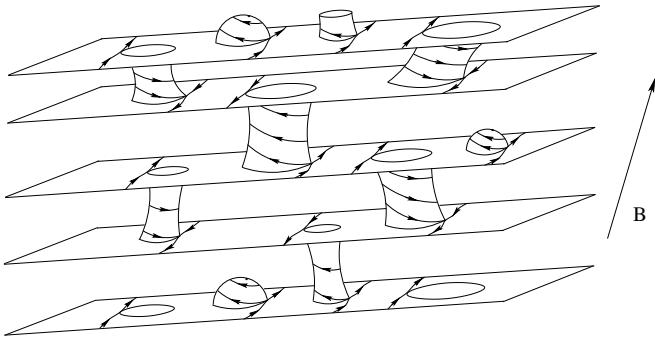


FIG. 5: A schematic representation of a complex Fermi surface carrying stable open trajectories of system (I.1).

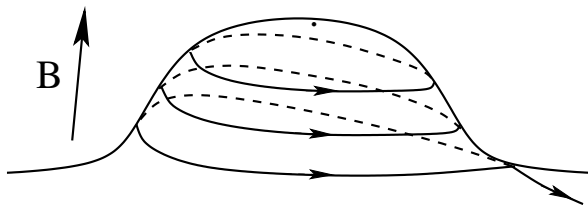


FIG. 6: A “simple” cylinder of closed trajectories that has a singular point of the system (I.1) as one of its bases.

Open trajectories of system (I.1) are defined by intersections of the carriers of open trajectories with planes orthogonal to \mathbf{B} . The described structure of the Fermi surface allows us to specify the most important properties of stable open trajectories in \mathbf{p} -space. Namely,

- 1) Each stable open trajectory of system (I.1) in \mathbf{p} -space lies in a straight strip of finite width in some plane orthogonal to \mathbf{B} (Fig. 7), passing through it (see [13, 14]).
- 2) All stable open trajectories for a given direction of \mathbf{B} have the same mean direction, given by the intersection of the plane orthogonal to \mathbf{B} , and some (constant for a given Stability Zone Ω) integral (i.e. generated by two reciprocal lattice vectors) plane Γ .

The indicated properties of stable open trajectories play a crucial role in the behavior of the conductivity of normal metals in sufficiently strong magnetic fields. In particular, the directions of the integral planes Γ_α , defined for different Stability Zones Ω_α , play the role of integer topological invariants observed in conductivity in strong magnetic fields ([22, 23]). The corresponding directions can actually be given by irreducible triples of integers $(M_\alpha^1, M_\alpha^2, M_\alpha^3)$, which can be called topological numbers observable in the conductivity of normal metals.

The topological representation of the Fermi surface in the form shown at Fig. 5 is not the only one, in particu-

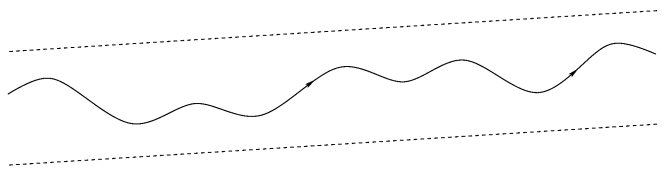


FIG. 7: The form of a stable open trajectory of system (I.1) in a plane orthogonal to \mathbf{B} .

lar, such representations are different for different Stability Zones Ω_α . It is easy to see that the specific structure of representation of the Fermi surface in this form (as well as the numbers $(M_\alpha^1, M_\alpha^2, M_\alpha^3)$) is determined by specifying cylinders of closed trajectories on the Fermi surface.

Thus, we can see that determination of the set \mathcal{M} of cylinders of closed trajectories completely determines the topology of the system (I.1) on the Fermi surface in the described situation. Strictly speaking, the complete description of trajectories of (I.1) also includes the rotation number on two-dimensional tori \mathbb{T}^2 (or the mean direction of open trajectories in \mathbf{p} -space), which are not defined just by the topology of division of the Fermi surface into the described components, but are easily calculated in the described situation for any given direction of \mathbf{B} ($\mathbf{B}/B \in \Omega_\alpha$). As we will show in the next chapter, the appearance of stable open trajectories on the Fermi surface actually entails the existence of a large set of directions of \mathbf{B} , for which special extremal closed trajectories of interest to us arise.

We note at once that stable open trajectories are not the only type of open trajectories that can arise on rather complex Fermi surfaces (see [15, 18, 19]). It can be noted, however, that in this case too, a change in the structure of the trajectories of system (I.1) is always associated with the appearance or disappearance of cylinders of closed trajectories and, in a sense, the presence of the set \mathcal{M} (or its absence), as well as its structure, determines the complete topological structure of the system (I.1) on the Fermi surface. Different questions related to the classification of open trajectories of the system (I.1), including their physical applications, as well as studies of the structure of unstable open trajectories of various types, can be found in [24–42]. It is also natural to note that the set \mathcal{M} determines the structure of the system (I.1) on the Fermi surface also if only closed trajectories appear on it, since in this case it contains information about all trajectories of the system (I.1). In any case, any change in the topological structure of the system (I.1) on the Fermi surface is always associated with the restructuring of the set \mathcal{M} and, in particular, with the disappearance or appearance of individual cylinders of closed trajectories.

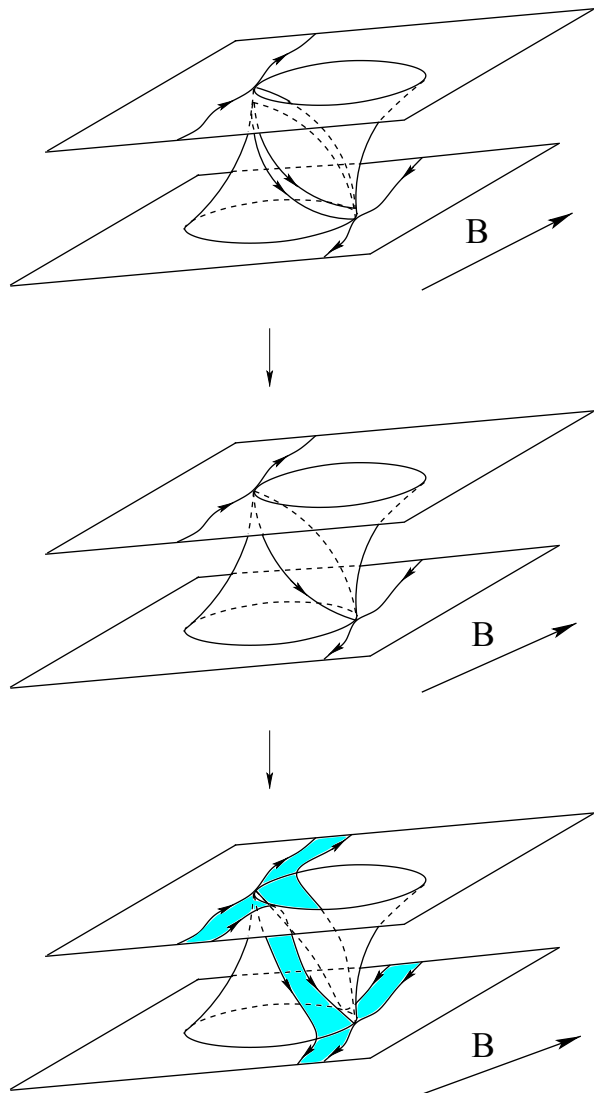


FIG. 8: The disappearance of a cylinder of closed trajectories on the Fermi surface during the rotation of the direction of \mathbf{B} .

III. RECONSTRUCTIONS OF THE STRUCTURE OF SYSTEM (I.1) AND THE APPEARANCE OF SPECIAL CLOSED TRAJECTORIES ON THE FERMI SURFACE

As we said above, a change in the structure of the system (I.1) is always associated with the disappearance or appearance of cylinders of closed trajectories on the Fermi surface. A scheme of the disappearance (or appearance) of one of these cylinders is shown at Fig. 8. It can be seen that with a correctly selected rotation of the direction of \mathbf{B} , the height of the cylinder of closed trajectories decreases, then vanishes and then a narrow strip appears in which jumps of the trajectories between the former bases of the cylinder become possible.

Thus, it can be seen that a change in the topologi-

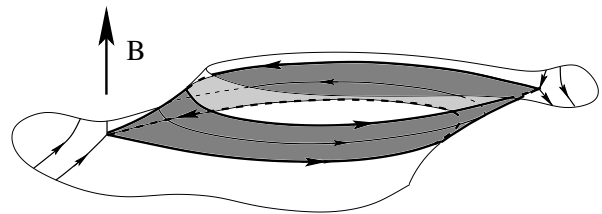


FIG. 9: A cylinder of closed trajectories of small height that accompanies a change in the topological structure of the system (I.1) on the Fermi surface.

cal structure of the system (I.1) is always accompanied by the appearance of a cylinder of closed trajectories of very small height, bounded by singular trajectories on their bases (Fig. 9). The period of rotation along closed trajectories tends to infinity when approaching the bases of the cylinder (singular trajectories) and, thus, must have a minimum on some trajectory inside the cylinder. The corresponding trajectory is “extremal”, in particular, when considering the phenomenon of cyclotron resonance, since the main oscillating terms in the intensity of absorption of microwave radiation come precisely from such trajectories. In this paper, we will be interested in precisely such trajectories. For convenience, we will call them special extremal trajectories. Most often (for example, for reconstructions near the boundaries of the regions where stable open trajectories appear on Fermi surfaces of not too large genus), such cylinders are centrally symmetric and then, if the extremal trajectory is unique (only this simplest case will be considered), it also has a central symmetry. In special cases, however, cylinders of closed trajectories can also appear in pairs and pass into each other under transformations of central symmetry. In this case, both cylinders of closed trajectories and extremal trajectories on them are not required to possess central symmetry. As we will see below, the presence of central symmetry of extremal trajectories provides a particularly convenient tool for studying the Fermi surface in the situation under consideration.

The period T of rotation along an extremal trajectory also tends to infinity (according to the logarithmic law) as the height h of the cylinder of closed trajectories tends to zero. The relatively slow growth of T in this case, however, allows us to maintain the condition $T/\tau \ll 1$ and, thus, to observe oscillation phenomena on such trajectories up to very small deviations of \mathbf{B} from the boundary of the reconstruction of the topological structure of the system (I.1). It can be seen, therefore, that the study of oscillation phenomena can serve as a very good tool for determining the boundaries of the reconstructions of the topological structure of system (I.1) on the Fermi surface. An exact study of the boundaries of the reconstructions of the system (I.1) (at the angular diagram), in turn, can serve as a good tool for refining the shape of the Fermi surface and other dispersion relation parameters $\epsilon(\mathbf{p})$ for metals with complex Fermi surfaces.

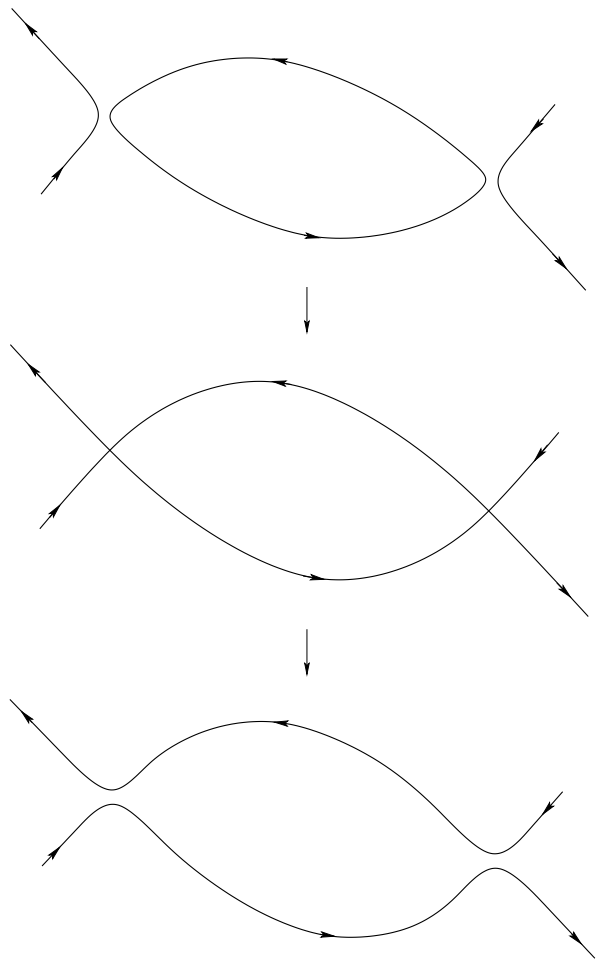


FIG. 10: Reconstruction of the extremal trajectory with a change in the topological structure of the system (I.1) on the Fermi surface.

The reason for the increase in the period T when the height of h tends to zero is the presence of points on an extremal trajectory very close to saddle singular points in \mathbf{p} -space, associated with the reconstruction of this trajectory when changing the structure of the system (I.1) (Fig. 10). It is near these points that the electron is delayed for a long time, running through the remaining sections of the trajectory rather quickly. When observing the phenomenon of cyclotron resonance, in particular, we will be interested in a situation where these points correspond to parts of the trajectory lying near the surface (inside the skin layer) of the sample under study, which, as we will see, leads to certain special features in the behavior of the oscillations of absorption of incident radiation.

As we can see, the extremal trajectory exists only until the corresponding cylinder of closed trajectories disappears and breaks up into other trajectories after that. The resulting trajectories after reconstruction (Fig. 10) could a priori be both open and closed. As we will see

later, however, whenever a change in the topological structure of the system (I.1) is associated with the appearance of open trajectories, it is more complex and requires, as a rule, an infinite number of reconstructions presented above.

As we noted above, this circumstance makes it natural to draw a connection between the angular diagrams describing the reconstructions of the topological structure of (I.1) with the angular diagrams describing the behavior of magnetoconductivity in metals in strong magnetic fields. Traditionally, angular diagrams for magnetoconductivity in conductors describe different conductivity behavior for different directions of \mathbf{B} , due to the appearance of various types of trajectories of the system (I.1) on the Fermi surface. In a somewhat simplified formulation, we can say that the main goal of the angular diagram of magnetoconductivity is to separate the directions of \mathbf{B} , corresponding to the “trivial” behavior of the conductivity (the presence of only closed trajectories on the Fermi surface), and the directions corresponding to “non-trivial” behavior (the appearance of open trajectories). The main thing in the structure of the angular diagram for conductivity in strong magnetic fields is, therefore, the indication of areas (on the unit sphere) of the directions of \mathbf{B} , corresponding to the presence of only closed trajectories on the Fermi surface, as well as a description of the set of directions of \mathbf{B} , corresponding to the appearance of open trajectories of various types. Thus, the angular diagram for magnetoconductivity in the general case contains regions (Stability Zones) corresponding to the appearance of stable open trajectories of the system (I.1) on the Fermi surface, as well as additional sets (one-dimensional curves or points) corresponding to the appearance of various types of unstable trajectories.

The angular diagram describing the reconstructions of the topological structure of the system (I.1) on the Fermi surface, according to our definition, represents the structure (a net of one-dimensional directions) of the set of directions of \mathbf{B} corresponding to reconstructions of the system of cylinders of closed trajectories on the Fermi surface. It can be seen, however, that such a diagram should include the structure of diagram for magnetoconductivity as part of its overall structure. The reason for this, as we already noted above, is that when approaching the directions of \mathbf{B} corresponding to the appearance of open trajectories, multiple reconstructions of closed trajectories must occur, giving in the limit the appearance of open trajectories of the system (I.1). As an example, we can consider the simplest diagrams that arise for a Fermi surface of the type of “corrugated cylinder” (Fig. 11). It is easy to see that the angular diagram of conductivity represents here the unit sphere with only one distinguished large circle (the “equator”) corresponding to the appearance of (unstable) periodic trajectories of the system (I.1). The angular diagram describing the reconstructions of the topological structure of the system (I.1) is more complicated and contains an infinite number of circles on S^2 , concentrating near the equator (Fig.

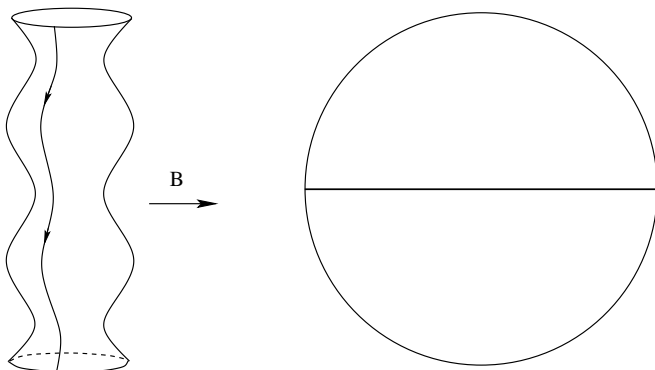


FIG. 11: Periodic trajectory and the conductivity diagram for a Fermi surface of the “corrugated cylinder” type.

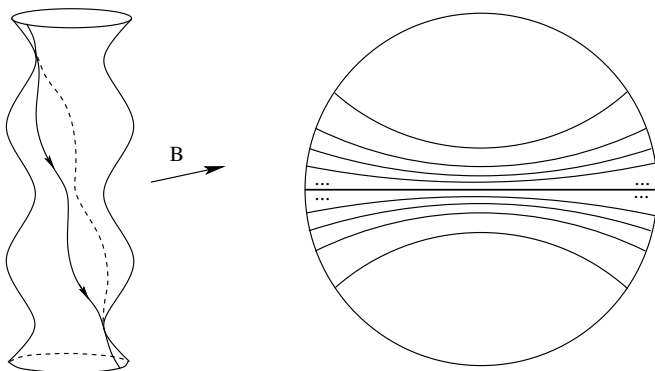


FIG. 12: An example of reconstruction of the topological structure of the system (I.1) and the angular diagram describing the reconstructions of the structure of (I.1) for a “corrugated cylinder” type Fermi surface.

12).

In general, the complexity of the angular diagrams describing the reconstructions of the topological structure of the system (I.1) can be very different, and, as follows from the above arguments, their complexity is directly related to the complexity of the corresponding diagrams for magnetoconductivity.

It is easy to give examples where both the second and first diagrams are simply trivial (do not contain any elements), as, for example, for a Fermi surface close to a sphere. In general, angular diagrams for magnetoconductivity can be divided into several complexity classes (see, for example, [43]). The simplest ones include naturally trivial diagrams corresponding to Fermi surfaces that do not allow the appearance of open trajectories at any direction of \mathbf{B} . The angular diagrams describing the reconstructions of the topological structure of the system (I.1) are not required to be trivial here, thus, it is easy to construct examples of the Fermi surfaces on which the reconstructions of the structure of (I.1) occur, but no open

trajectories appear. The diagrams describing the reconstructions of the topological structure of the system (I.1) contain in this case a finite net of one-dimensional directions of \mathbf{B} (on \mathbb{S}^2) corresponding to the appearance of the “cylinders of zero height” described above.

The second class of angle diagrams for magnetoconductivity is represented by angular diagrams containing a net of one-dimensional curves on \mathbb{S}^2 , corresponding to the appearance of (unstable) periodic open trajectories on the Fermi surface. As can be seen from the example presented above, the angular diagrams describing the reconstructions of the topological structure of the system (I.1) are in this case more complex and contain an infinite number of one-dimensional curves corresponding to the appearance of “cylinders of zero height” in the generic case.

The most complex diagrams for magnetoconductivity include diagrams containing nontrivial regions of existence of open trajectories of the system (I.1) (stable open trajectories). In fact (see [43]), such diagrams can also be divided into two classes differing in level of complexity. As we will see below, the angular diagrams describing the reconstructions of the topological structure of the system (I.1) are in this case the most complex and have a very rich structure.

In this paper, we would like, in particular, to provide a schematic description of the set of all directions of \mathbf{B} , corresponding to the reconstructions of the system (I.1), on the angular diagrams of the most general, and, in particular, quite complex, type (containing at least one Stability Zone). We will need, among other things, to give a schematic description of the structure of this set near the boundary of one fixed Stability Zone Ω_α .

For this purpose, let us consider a “not too complicated” case when the Fermi surface has genus 3 and extends in all three directions in the \mathbf{p} -space. To simplify as much as possible the visual representation of the structure of such a surface for the direction of \mathbf{B} lying in one of the Stability Zones, one can imagine as an example the surface shown at Fig. 13. When the directions of \mathbf{B} are close to the vertical, it is easy to visually distinguish a pair of non-equivalent carriers of open trajectories (integral planes), as well as two different cylinders of closed trajectories that separate these carriers (“thick” and “thin” cylinders). Cylinders of closed trajectories have different types (“electron” and “hole”) and both have central symmetry in the described situation (the Stability Zone for a surface of genus 3, extending in three directions). The direction of \mathbf{B} lies within the Stability Zone as long as both cylinders at Fig. 13 contain non-singular closed trajectories of the system (I.1). The boundary of the Stability Zone Ω_α is determined by the disappearance of nonsingular closed trajectories on one of the cylinders (in this case, on the “thick” cylinder) shown at Fig. 8 (that is, the height of the corresponding cylinder of closed trajectories vanishes).

What can be said about the trajectories of the system (I.1) for directions of \mathbf{B} lying outside the Zone Ω_α in

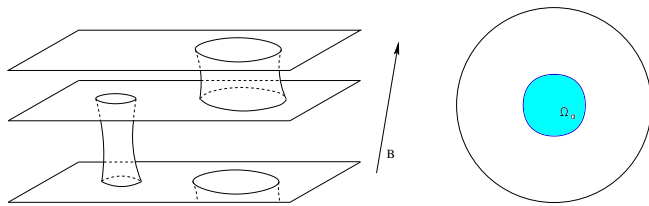


FIG. 13: A simplified representation of the structure of a Fermi surface, having a region of existence of stable open trajectories (a Stability Zone) in the full space of directions of \mathbf{B} (on the sphere \mathbb{S}^2).

the immediate vicinity of its boundary? One can see, in reality, that the described structure of the Fermi surface allows one to give a description of the trajectories of (I.1) for such directions as well. The reason for this is that, after crossing the boundary of Ω_α , non-singular closed trajectories remain on the second (“thin”) cylinder separating the carriers of open trajectories. As a result, the Fermi surface can now be represented as a union of pairwise “merged” former carriers of open trajectories, separated by cylinders of closed trajectories remaining on the “thin” cylinders. In such a situation, the system still retains the memory of the integral plane Γ_α , associated with the Zone Ω_α , which continues to play a significant role in the description of the trajectories of system (I.1) on the Fermi surface.

It is natural to divide the nonsingular trajectories arising for the directions of \mathbf{B} near the boundary of the Zone Ω_α into the trajectories lying on the “thin” cylinder and the trajectories, lying on a pair of “merged” carriers of open trajectories. It can be seen that the latter are either closed (if the plane orthogonal to \mathbf{B} intersects Γ_α in an irrational direction), or can be periodic (if the plane orthogonal to \mathbf{B} intersects Γ_α in an integer direction in \mathbf{p} -space). Both situations are shown schematically at Fig. 14, which shows the division of a pair of former carriers of open trajectories into cylinders of the formed closed trajectories (upper picture), or into cylinders of closed trajectories and layers of periodic trajectories in \mathbf{p} -space (bottom picture). As one can see, in the first case, exactly three nonequivalent cylinders of closed trajectories appear on a pair of former carriers, and in the second case - exactly one cylinder of closed trajectories (and two nonequivalent layers of periodic trajectories - one on the “upper” and one on the “lower” carrier). It can be seen, therefore, that in the situation under consideration, each of the cylinders of closed trajectories can only go into itself under the transformation $\mathbf{p} \rightarrow -\mathbf{p}$ and, therefore, possess central symmetry. As we have already said, extremal closed trajectories with such symmetry will be of particular interest to us in studying the Fermi surface.

It should be said right away that the appearance of periodic trajectories near the boundary of Ω_α occurs only for non-generic directions of \mathbf{B} (the intersection of the plane orthogonal to \mathbf{B} and Γ_α represents a reciprocal

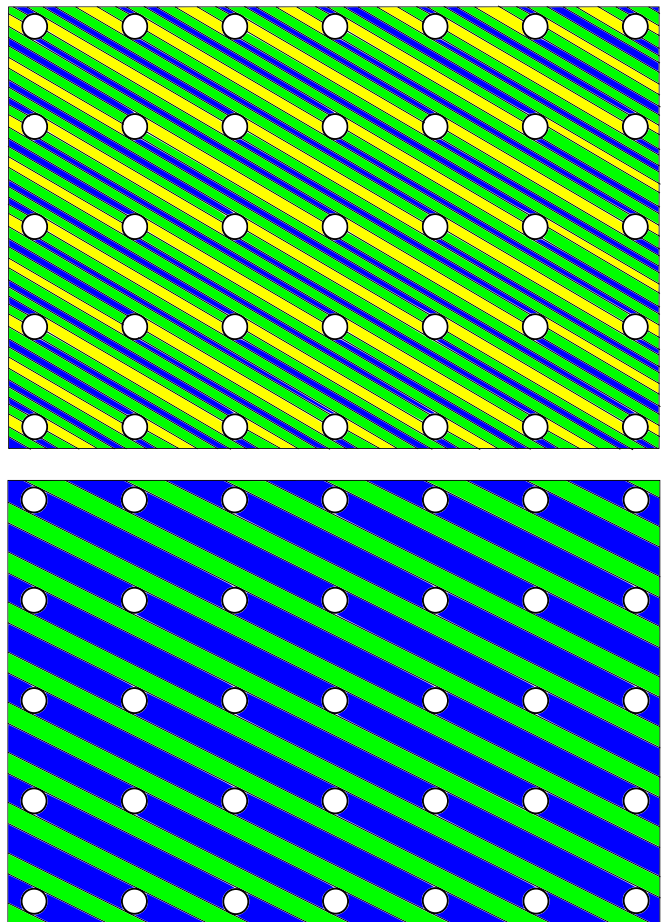


FIG. 14: A pair of former carriers of open trajectories (periodically deformed integral planes) carrying either closed trajectories or closed and periodic trajectories after crossing the boundary of Ω_α . The circles indicate the places where the trajectory jumps from the “upper” carrier to the “lower” and vice versa.

lattice vector). It is easy to show that the corresponding directions of \mathbf{B} form an infinite set of segments adjacent to the boundary of Ω_α , the length of which decreases rapidly with increasing module of the corresponding integer vector in \mathbf{p} -space. For integer vectors of a small module, the corresponding segments can reach another Stability Zone and have no endpoints. Such segments are, in fact, extensions of segments passing through the entire Stability Zone and corresponding to the appearance of periodic trajectories on the Fermi surface (Fig. 15). (We note here that sometimes in the literature one can find the statement that open trajectories on the Fermi surface become periodic if the plane orthogonal to \mathbf{B} contains an integer (rational) direction. Such a statement, generally speaking, is false. To formulate a more correct statement, we must first note that if we consider a change in stable open trajectories, then the direction of \mathbf{B} belongs to some Stability Zone Ω_α corresponding to a certain integral plane Γ_α . In this case, stable

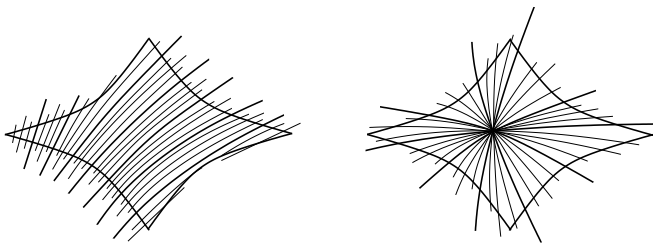


FIG. 15: Stability Zones and special segments corresponding to the appearance of periodic trajectories on the Fermi surface.

open trajectories become periodic if and only if the intersection of the plane orthogonal to \mathbf{B} and the plane Γ_α has a rational (integer) direction, i.e. if the plane orthogonal to \mathbf{B} contains an integer direction that also belongs to the corresponding plane Γ_α . It can be seen, therefore, that the appearance of periodic open trajectories among stable open trajectories is directly related to the structure of the system (I.1) described above and, in fact, is closely connected with the topological numbers ($M_1^\alpha, M_2^\alpha, M_3^\alpha$).

The length of the arising closed trajectories is inversely proportional to the probability of “hopping” of the trajectory from one carrier to another and the smaller the farther the direction of \mathbf{B} from the boundary of the Zone Ω_α . In the immediate vicinity of the boundary of Ω_α for generic directions of \mathbf{B} the length of the corresponding cylinders of closed trajectories is very long (see Fig. 16) and goes to infinity on the border itself. Closed trajectories arising on such cylinders also have a rather large length and a somewhat specific shape (Fig. 17) when approaching the boundary Ω_α . In particular, in the immediate vicinity of the boundary of Ω_α , the condition $T/\tau \ll 1$ must be violated and the corresponding long closed trajectories become indistinguishable from open from an experimental point of view. As one of the consequences of this, the behavior of conductivity in strong magnetic fields for the corresponding directions of \mathbf{B} also becomes quite complicated and may not be described by simple asymptotic formulas even for fairly large values of B (see e.g. [44]). As indicated in [45], to determine the exact mathematical boundaries of the Stability Zones, it might be better to actually use observations of oscillation phenomena in strong magnetic fields that track the reconstructions of the topological structure of the system (I.1) at the boundaries of Ω_α (the disappearance of a cylinder of “short” closed trajectories), which we consider here. It can be noted that during the experimental observation of oscillation phenomena in this situation, it is specific that one of the oscillating terms disappears when crossing the boundary of the Stability Zone from the inside without other oscillating terms appearing immediately due to the large length of new closed trajectories near the boundary of Ω_α . When moving away from the boundary of Ω_α , the lengths of the corresponding trajectories, however,

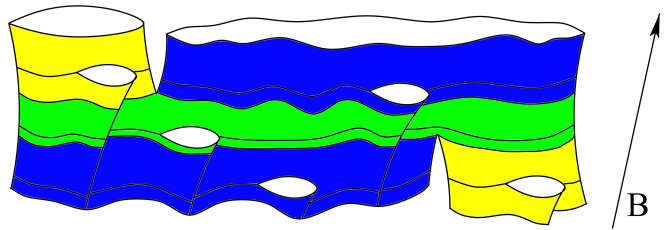


FIG. 16: Cylinders of closed trajectories arising on a pair of former carriers of open trajectories after crossing the boundary of a Stability Zone at an angular diagram.

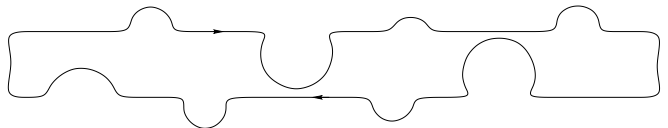


FIG. 17: Long closed trajectories arising on a pair of former carriers of open trajectories in the immediate vicinity of the boundary of a Stability Zone.

decrease rather quickly, and the trajectories themselves take on a “normal” shape. As a consequence of this, in the oscillation picture, it also becomes possible to observe the oscillation terms corresponding to the new cylinders of closed trajectories.

A somewhat different situation is observed if we approach (or move away) the boundary of a Zone Ω_α along one of the adjacent segments corresponding to the appearance of periodic trajectories. In this case, as can be seen (Fig. 14, lower picture), the length of the cylinder of closed trajectories remains unchanged when moving along a given segment. However, its height increases rapidly (and the width of the layers of periodic trajectories decreases) with distance from the boundary of Ω_α , which is associated with an increase in the probability of hopping between former carriers of open trajectories (diameter of circles at Fig. 14). It can also be noted here that in this case the cylinders of closed trajectories are not generic, since they contain two singular points on each of their bases. The corresponding topological structure of the system (I.1) is also, therefore, not a generic structure and arises only for a set of measure zero at the angular diagram. At the end point of the segment, the width of the layers of periodic trajectories vanishes and the former carriers of open trajectories completely disintegrate into cylinders of closed trajectories (Fig. 14, upper picture). The corresponding reconstruction of the topological structure of (I.1) should also be attributed to non-generic reconstructions observed only at isolated points (and not along one-dimensional curves) at the angular diagram.

Here, of course, it should be noted that the boundaries of the Stability Zones Ω_α (as well as the special seg-

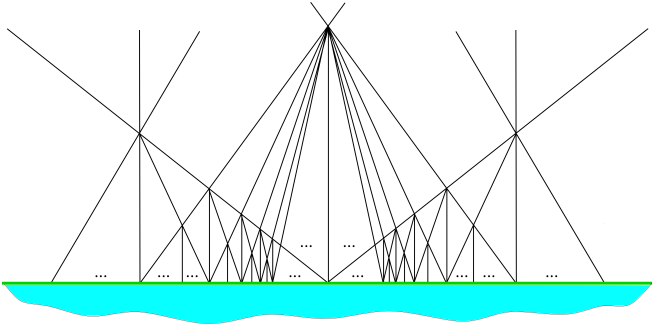


FIG. 18: The net of directions of \mathbf{B} , corresponding to the reconstructions of the structure of the system (I.1) near the boundary of a Stability Zone Ω_α (very schematically).

ments adjoining them) are completely special sets from the point of view of our definition of a change of the structure of system (I.1) on the Fermi surface. On the one hand, as we have already seen, the boundary of a Zone Ω_α itself is determined by the described reconstruction with the disappearance of a cylinder of closed trajectories. When approaching the boundary of Ω_α from inside the topological structure of the system (I.1) does not change. When approaching the boundary of Ω_α from the outside, however, there is an infinite number of reconstructions of the system (I.1) on the Fermi surface, so we can not say which structure has (I.1) near the boundary of Ω_α . A similar pattern is also observed when approaching special segments (outside the Zone Ω_α) corresponding to the appearance of periodic trajectories on the Fermi surface.

The reconstructions of cylinders of closed trajectories on the former carriers of open trajectories represent changes in the topological structure of the system (I.1) on the Fermi surface and are always accompanied by the disappearance (and the appearance of new ones) of such cylinders. Such reconstructions occur on certain lines at the angular diagram (see [46]), whose density tends to infinity when approaching the boundary of a Zone Ω_α , as well as the special segments corresponding to the appearance of periodic trajectories. When moving away from the boundary of the Zone Ω_α , as well as the special segments described above, the density of the “net” of directions of \mathbf{B} corresponding to the reconstructions of the structure of (I.1) is decreasing. Very schematically, the net of directions of \mathbf{B} , corresponding to the reconstructions of the structure of (I.1) near the boundary of Ω_α , can be represented by Fig. 18.

The given situation (the ability to describe the trajectories of the system (I.1)) persists until closed trajectories disappear on the second (“thin”) cylinder connecting pairs of former carriers of open trajectories (Fig. 13). It can be seen, therefore, that along with the “first” boundary of a Stability Zone Ω_α it is to some extent natural to introduce its second boundary (see [46]), which defines the “area of influence” Σ_α of the Zone Ω_α at the

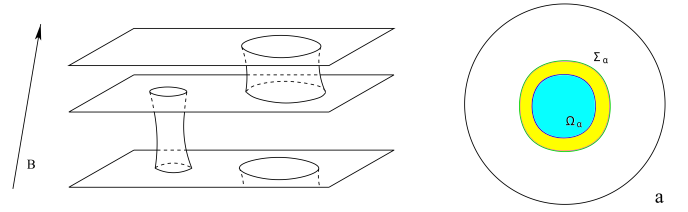


FIG. 19: The first and second boundaries of a Stability Zone on the angular diagram.

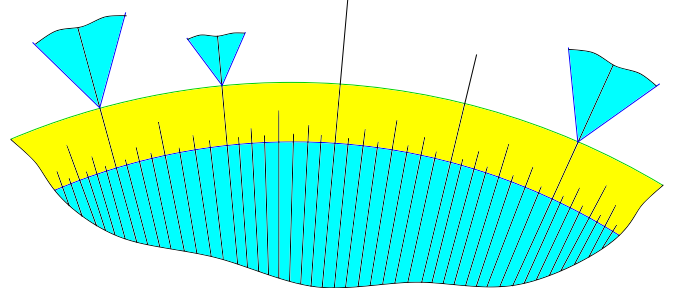


FIG. 20: Typical structure of the section of the second boundary of a Stability Zone Ω_α on the angular diagram (schematically).

angular diagram (Fig. 19). The domain $\Omega'_\alpha = \Sigma_\alpha \setminus \Omega_\alpha$ can naturally be called the derivative of the Zone Ω_α , since the structure of the system (I.1) for the corresponding directions of \mathbf{B} is directly related to the structure of this system in the Zone Ω_α . Unlike the Stability Zones Ω_α themselves, the derivatives of two different Stability Zones $\Omega'_\alpha, \Omega'_\beta$ may intersect with each other. In addition, unlike the first boundaries of the Stability Zones, the second boundaries are not such a complex set from the point of view of reconstructions of the structure of system (I.1) and everywhere, with the exception of only a finite number of points, are described by a simple (elementary) reconstruction of this structure. The only exceptions are certain points of the second boundary (Fig. 20), where it can be crossed by the segments that correspond to the appearance of periodic trajectories, as well as other Stability Zones (see [43]).

One can see, therefore, that the set of directions of \mathbf{B} , corresponding to reconstructions of the topological structure of the system (I.1), is rather rich for fairly complex Fermi surfaces. So, the presence of only one Stability Zone on the angular diagram entails in fact the existence of a rather complex net of one-dimensional curves on \mathbb{S}^2 , corresponding to changes in the set \mathcal{M} with the height of one of the cylinders of closed trajectories turning to zero. First of all, it is interesting to study here the oscillation phenomena at the first and second boundaries of the Zone Ω_α , which actually help to determine their exact location. No less interesting for studying the Fermi

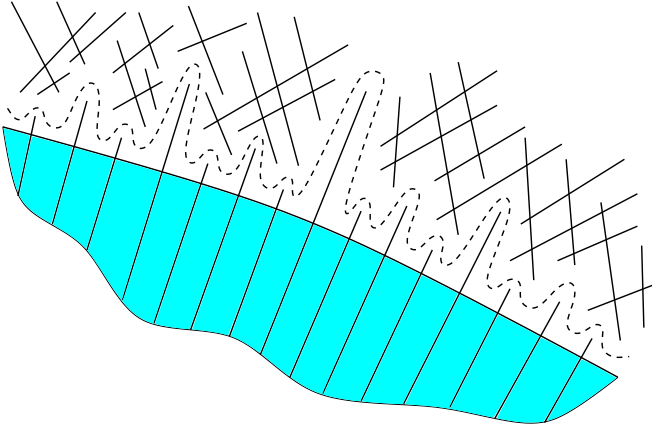


FIG. 21: The set (net) of experimentally observed directions of \mathbf{B} near the boundary of a Stability Zone corresponding to reconstructions of the structure of system (I.1) on the Fermi surface (schematically).

surface, however, is also the net of directions of \mathbf{B} between the first and second boundaries of the Stability Zone, which is associated with the reconstructions of the structure of system (I.1) on the former carriers of open trajectories. As mentioned above, to study the features of oscillation phenomena that are interesting to us, the corresponding directions of \mathbf{B} should not approach too close to the first boundary of the Zone Ω_α or the adjacent segments corresponding to the appearance of periodic trajectories on the Fermi surface. From the point of view of modern experimental capabilities (for producing strong magnetic fields and materials with big electron mean free path), however, these restrictions are not really too strong and leave a significant part of this structure available for study (Fig. 21).

It can also be noted here that the described structure of the regions Ω_α and Σ_α is, in a sense, the simplest. For example, there may be cases when the first and second boundaries of a Zone Ω_α are “composite”, and the corresponding region Ω'_α is not connected (see e.g. Fig. 22). In addition, surfaces of a large genus can have a larger number of cylinders separating carriers of open trajectories (and even a larger number of pairs of carriers of open trajectories). Nevertheless, all the above remarks related to the topological structure of the trajectories near the Stability Zones are retained for more complex cases (see, for example, [46]) and, in particular, an increase in the number of Stability Zones at the angular diagram leads in general case to rapid increase in the set of directions of \mathbf{B} , corresponding to reconstructions of the topological structure of system (I.1) on the Fermi surface.

Thus, for conductivity diagrams, the complexity of which is limited by the presence of Stability Zones (and segments corresponding to the appearance of periodic trajectories), the set of directions of \mathbf{B} corresponding to reconstructions of the topological structure of (I.1) al-

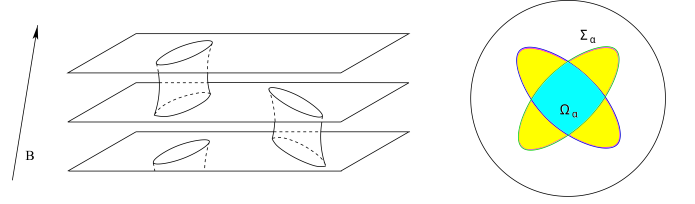


FIG. 22: An example of a model Fermi surface having a Stability Zone with composite first and second boundaries.

ways includes the boundaries of the Stability Zones, as well as a rather rich “net” of one-dimensional directions of \mathbf{B} in the space between the Zones. The indicated net of one-dimensional directions of \mathbf{B} on \mathbb{S}^2 unlimitedly condenses near the boundaries of the Stability Zones, as well as the segments adjacent to them, corresponding to the appearance of periodic trajectories on Fermi surface. Observation of oscillatory phenomena corresponding to the reconstructions of the structure of (I.1) is possible on this net of directions with not too close approach to the boundaries of the Stability Zones or adjacent segments, as well as at the boundaries of the Zones Ω_α when approaching them from the inside.

The sets of the directions of \mathbf{B} described above are directly connected with the Stability Zones and, in particular, are associated with reconstructions of the structure of (I.1) on the former carriers of open trajectories. At the same time, additional reconstructions of the structure of system (I.1) that are not related to carriers of open trajectories (occurring on other parts of the Fermi surface) and, therefore, not related to these reconstructions, can occur on Fermi surfaces of a sufficiently large genus. The corresponding structure is not connected with the above structure and the corresponding nets of directions of \mathbf{B} in this case “overlap” the sets of directions described above, in particular, they can lie inside the Zones Ω_α and intersect with their boundaries.

As follows from the consideration of the general complexity classes of angular diagrams of magnetoconductivity in metals (see [43]), angular diagrams corresponding to the appearance of only stable and periodic trajectories on the Fermi surface (complex diagrams of type A) represent a separate class of complex angular diagrams. As follows from general considerations, the appearance of complex diagrams of type A is apparently much more likely than the appearance of complex diagrams of the other class (complex diagrams of type B) even for conductors with very complex Fermi surfaces. Diagrams of type A contain in generic case a finite number of Stability Zones and the above picture of the set of directions of \mathbf{B} corresponding to the reconstructions of the structure of system (I.1) on the Fermi surface is common to diagrams of this type.

Complex diagrams of the second type (type B) can be defined as diagrams containing directions of \mathbf{B} corresponding to the appearance of more complex (chaotic)

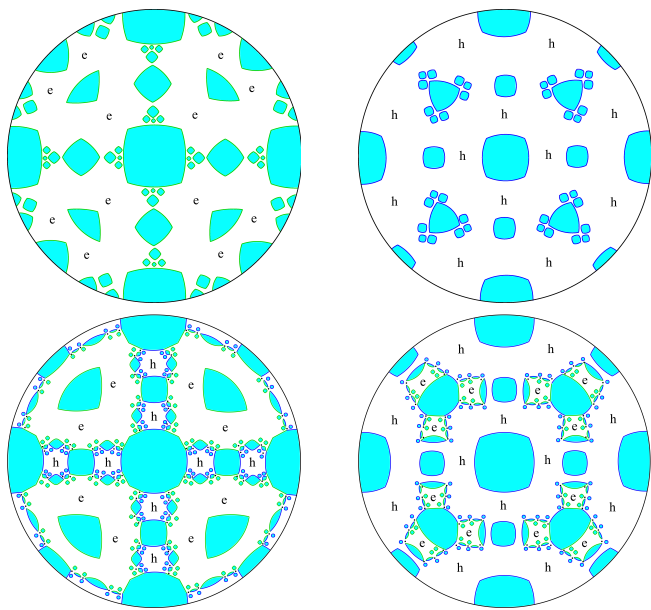


FIG. 23: Diagrams of type A (above) and B (below). The letters e and h denote the regions of electron and hole Hall conductivity in the absence of open trajectories on the Fermi surface. (Very schematically, only the Stability Zones and directions of \mathbf{B} , corresponding to the appearance of “chaotic” trajectories on the Fermi surface are shown).

unstable trajectories on the Fermi surface. In fact, as follows from the general consideration (see [43, 46]), diagrams of this type contain, in addition, an infinite number of Stability Zones in the generic case, and also differ from diagrams of type A by special behavior of Hall conductivity (alternating areas of electron and hole conductivity) in areas corresponding to the presence of only closed trajectories on the Fermi surface (Fig. 23).

Thus, for the most complex Fermi surfaces (namely, surfaces on which trajectories that are more complex than stable and periodic open trajectories can appear), the structure of the set of directions of \mathbf{B} that correspond to reconstructions of the topological structure of the system (I.1) will be especially rich. In particular, the conductivity angular diagrams for such Fermi surfaces contain, in the generic case, an infinite number of Stability Zones that have condensation points corresponding to the special directions of \mathbf{B} , connected with the appearance of especially complex (chaotic) trajectories on the Fermi surface. Near such directions of \mathbf{B} , the structure of the indicated set (as well as the structure of the system (I.1) on the Fermi surface) becomes especially complicated. As in the case of approaching the boundaries of the Stability Zones Ω_α , approaching the special directions of \mathbf{B} , corresponding to the appearance of chaotic trajectories, requires an infinite number of “elementary acts” of reconstruction of the structure of system (I.1). For the rest, as regards the general features of the set of directions of \mathbf{B} , corresponding to changes in the topological structure of (I.1), their description here contains

the same basic details as for diagrams of type A.

IV. ELEMENTARY RECONSTRUCTIONS OF THE STRUCTURE OF SYSTEM (I.1) AND THE APPEARANCE OF SPECIAL CLOSED TRAJECTORIES ON THE FERMI SURFACE.

Based on the above picture, we can see that, in addition to the boundaries of the Stability Zones Ω_α , available to experimental study reconstructions of the structure of the system (I.1) occur either in areas that correspond to the presence of only closed trajectories on the Fermi surface, or also inside the Stability Zones, without being associated with the appearance or disappearance of open trajectories. Such reconstructions can be called “elementary” and correspond to the disappearance (appearance) of cylinders of closed trajectories on both sides of the curve (on \mathbb{S}^2) that separates two different structures of the system (I.1). Oscillation phenomena that indicate the corresponding reconstruction of the structure of (I.1) must be observed on both sides of such a curve, so we must record the change of some oscillation terms by others at its intersection. In this chapter, we will look in more detail at the types of elementary reconstructions of the structure of system (I.1) and discuss the probability of their occurrence on real Fermi surfaces.

As we mentioned above, the bases of the cylinders of closed trajectories contain a saddle singular point of the system (I.1) and can take one of the forms shown at Fig. 24. At the time of the reconstruction of the topological structure of system (I.1), we must observe the appearance of a “cylinder of zero height”, which represents actually two singular points connected by a set of singular trajectories.

Apparently, the most frequent type of the reconstruction of the structure of (I.1) is the reconstruction shown at Fig. 25. Fig. 26 represents the main components of the disappearing and appearing cylinders of closed trajectories (namely, their upper and lower bases, as well as the extremal trajectories arising on them), and the structure of the “cylinder of zero height” arising at the time of reconstruction. It is easy to see that the reconstruction shown at Fig. 25, leads to the disappearance of exactly one cylinder of closed trajectories and the appearance of exactly one new cylinder.

In the general case, for generic reconstructions, the corresponding “cylinder of zero height” contains exactly two singular points of the system (I.1) connected by singular trajectories (we will not consider here special “degenerate” cases with a larger number of singular points). We will consider both singular points on a “cylinder of zero height” to be non-degenerate (which corresponds to the non-zero value of the Gaussian curvature at the corresponding points on the Fermi surface), in particular, this means that exactly two singular trajectories of the system (I.1) enter and exit each such point. For elementary reconstructions of the structure of (I.1), all singular tra-

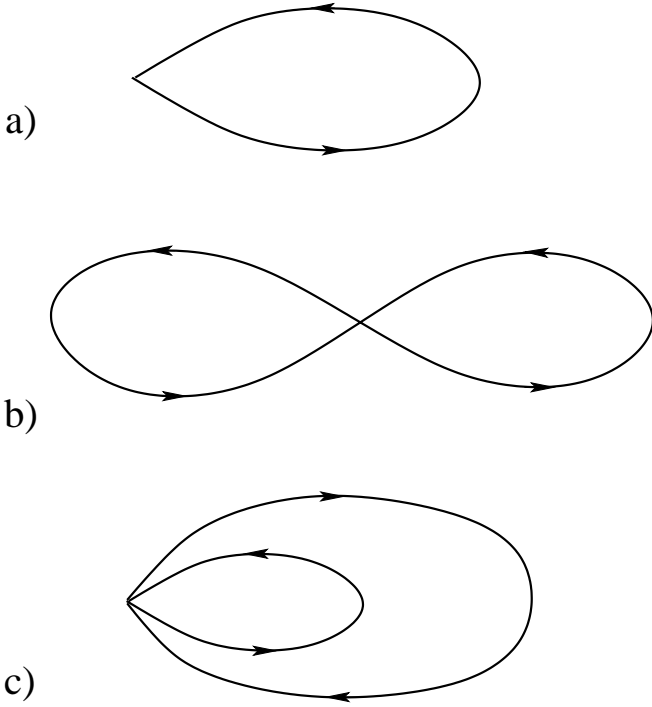


FIG. 24: Possible forms of bases of “nontrivial” cylinders of closed trajectories (in a plane orthogonal to \mathbf{B}).

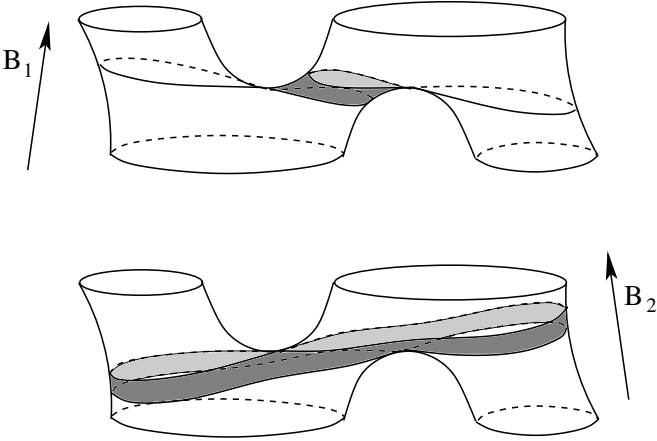


FIG. 25: The main type of “elementary” reconstruction of the structure of (I.1) (only the part of the Fermi surface on which the reconstruction takes place is shown).

jectories that exit from a pair of such points must also end at these points.

For Fermi surfaces of “moderate complexity” all the elements involved in the reconstruction shown at Fig. 25 have central symmetry. In particular, it is present in extremal trajectories arising on the disappearing and appearing cylinders of closed trajectories. As a relatively simple consideration of Fermi surfaces of the most vari-

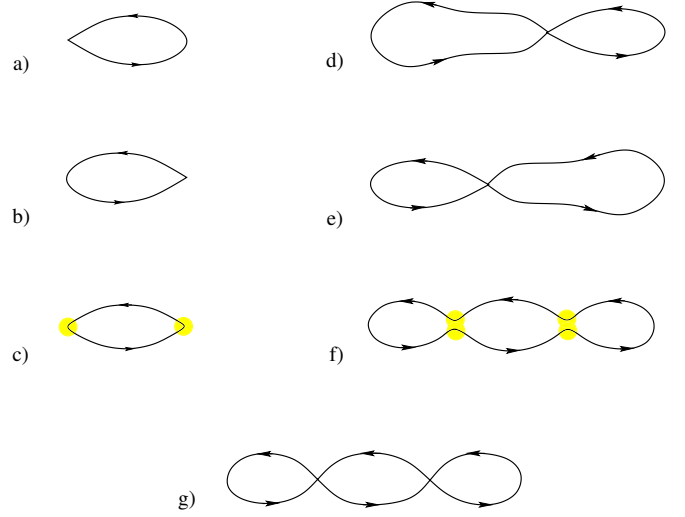


FIG. 26: The main elements involved in the reconstruction of the structure of system (I.1), shown at Fig. 25. The lower and upper bases of the disappearing cylinder of closed trajectories and the extremal trajectory arising on it (a-c). The lower and upper bases of the appearing cylinder of closed trajectories and the extremal trajectory arising on it (d-f). The “cylinder of zero height” that appears at the moment of reconstruction (g).

ous types shows, the type of “elementary” reconstruction shown at Fig. 25 - 26, takes place, in fact, in the vast majority of cases for real Fermi surfaces.

The topological type of reconstruction shown at Fig. 25 - 26, however, is not the only possible one. Fig. 27 and 28 show another type of reconstruction, different from the one shown at Fig. 25 and 26.

Here one can immediately note one important difference between the types of reconstruction shown at Fig. 25 - 26 and 27 - 28. Namely, the reconstruction shown at Fig. 25 - 26, can possess central symmetry and thus occur just on one part of the Fermi surface. As for the reconstruction shown at Fig. 27 - 28, it obviously cannot have a central symmetry and can thus only occur together with a similar reconstruction on another part of the Fermi surface that passes into this one under the central symmetry transformation. It can be seen, therefore, that for the reconstructions shown at Fig. 27 - 28, the corresponding Fermi surface must have rather significant complexity (have a sufficiently large genus) even among traditionally complex examples of Fermi surfaces.

In general, to enumerate the various topological types of “elementary” reconstructions of the structure of system (I.1) on the Fermi surface, it is actually enough to fix the topological structure of the “cylinder of zero height” in the plane orthogonal to \mathbf{B} and also indicate ways for splitting both saddle singular points with parallel displacement of this plane, for example, “up” (along the direction of the magnetic field). Fig. 29 shows possible schemes of such a description for the “cylinder of zero

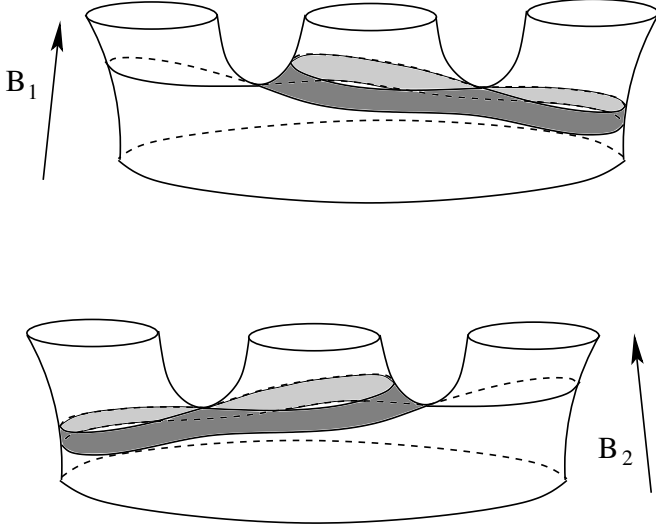


FIG. 27: An example of the reconstruction of the structure of system (I.1) on a part of the Fermi surface.

height”, corresponding to the examples shown at Fig. 25 - 26 and 27 - 28.

We note here that the direction of the arrows at Fig. 29 is somewhat arbitrary and should be reversed when replacing $\mathbf{B} \rightarrow -\mathbf{B}$. If we are only interested in changing the topology of the carriers of the trajectories on the indicated part of the Fermi surface, we can, in reality, not indicate these directions. Each of the schemes (a-d) shown at Fig. 29 fixes the structure of gluing to the “cylinder of zero height” other cylinders of closed trajectories “from above”. With a parallel shift of the plane orthogonal to \mathbf{B} “down” (against the direction of \mathbf{B}), the way of splitting each of the singular points changes to the opposite ($(a) \leftrightarrow (b)$, $(c) \leftrightarrow (d)$), which also fixes the structure of gluing to the “cylinder of zero height” other cylinders of closed trajectories “from below”.

In addition to fixing the structure of gluing to the “cylinder of zero height” of other cylinders of closed trajectories at the moment of reconstruction, the specified scheme of splitting singular points also defines the structure of the system (I.1) before and after it. Indeed, the reconstruction of the structure of (I.1) occurs at small rotations of the magnetic field direction, which entail corresponding rotations of the plane orthogonal to \mathbf{B} . Those rotations of \mathbf{B} , at which the singular points remain in this plane, correspond to the motion along the curve of the reconstruction of the structure of (I.1), and the rotations at which the singular points cannot simultaneously remain in the same plane, orthogonal to \mathbf{B} , correspond to the crossing this curve at the angular diagram. To monitor the reconstruction of the structure of (I.1), one can observe the rotation of the plane orthogonal to \mathbf{B} and containing some fixed point on the interval between two singular points. It is easy to see that during rota-

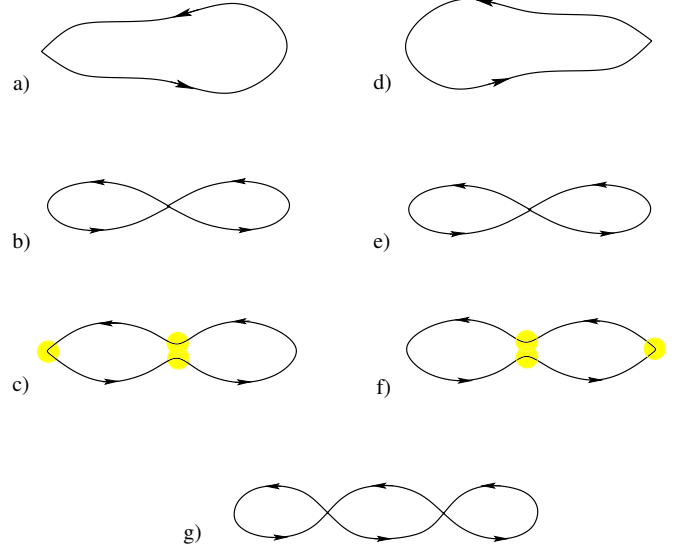


FIG. 28: The main elements involved in the reconstruction of the structure of system (I.1), shown at Fig. 27. The lower and upper bases of the disappearing cylinder of closed trajectories and the extremal trajectory arising on it (a-c). The lower and upper bases of the appearing cylinder of closed trajectories and the extremal trajectory arising on it (d-f). The “cylinder of zero height” that appears at the moment of reconstruction (g).

tions corresponding to a reconstruction of the structure of (I.1), such a plane goes upward near one of the singular points and downward near the other, and the rules for splitting the singular points in the rotating plane must comply with the rules specified initially. Then displacing the rotated plane parallel to itself and using the same fixed rules for reconstruction of trajectories as it passes through singular points, it is easy to restore the shape of the appearing (or disappearing) cylinders of closed trajectories of small height, as well as the structure of gluing to them other cylinders of closed trajectories before or after the reconstruction.

It can also be noted here that the terms “disappearing” and “appearing” structures are also arbitrary to some extent and depend on the direction of rotation of the magnetic field. Actually, it is more correct to speak of two different structures of the system (I.1) adjacent to each other along a line of reconstruction at the angular diagram. From this point of view, in particular, it can be seen, as above, that replacing the splitting rules at once for both singular points in the above-described scheme does not essentially change the topological type of reconstruction taking place on a fixed curve. One can therefore also say that to describe the topological types of reconstructions of the structure of system (I.1), it suffices to list the topological structures of the corresponding “cylinders of zero height” in the plane orthogonal to \mathbf{B} and indicate for each cylinder, whether the directions of the

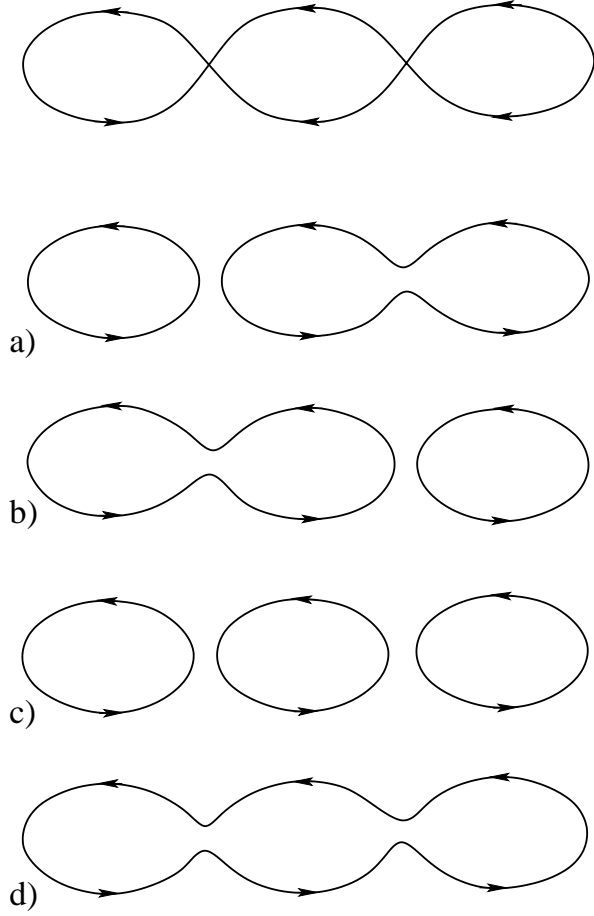


FIG. 29: “Cylinder of zero height”, corresponding to the examples shown at Fig. 25 - 26 and 27 - 28, and possible options for splitting singular points with a parallel shift of the corresponding plane, orthogonal to \mathbf{B} , in the direction of the magnetic field.

group velocity at singular points are co-directional or opposite to each other.

So, in particular, from this point of view, diagrams (a) and (b) at Fig. 29 correspond to the same topological type of reconstruction shown at Fig. 25 - 26, and diagrams (c) and (d) are of the topological type shown at Fig. 27 - 28. Fig. 30 presents all different types of “cylinders of zero height”, which can arise in elementary reconstructions of the structure of the system (I.1) on the Fermi surface. At Fig. 31 - 40 one can see the corresponding changes in the topological structure of the system (I.1) for different orientations of the group velocity at saddle singular points for cases other than those presented at Fig. 25 - 26 and 27 - 28.

Among the presented topological types of reconstructions of the structure of system (I.1) we can immediately distinguish cases of possible central symmetry of the corresponding section of the Fermi surface. It is easy to see that the presented sections of the Fermi surface cannot possess central symmetry if it is not possessed by

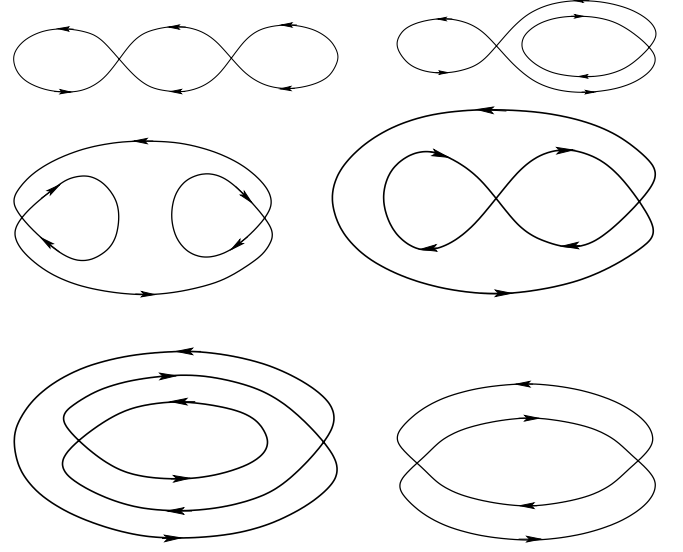


FIG. 30: Different types of “cylinders of zero height” arising at the moment of elementary reconstruction of the topological structure of the system (I.1) on the Fermi surface.

the corresponding “cylinders of zero height”. In addition, central symmetry cannot be observed also in those cases when the group velocities at the singular points on the “cylinder of zero height” are co-directed with each other. All the corresponding types of reconstructions of the system (I.1) can, therefore, arise only in pairs on the Fermi surface, which, in turn, requires its sufficient complexity.

It can be stated, therefore, that of the types of reconstruction presented at Fig. 31 - 40, only the reconstructions shown at Fig. 33 and 39 can have central symmetry. It is easy to see at the same time that the reconstruction shown at Fig. 39 leads to the disappearance of a pair of cylinders of closed trajectories and the appearance of a pair of new cylinders, which, in turn, also requires sufficient complexity of the Fermi surface.

To all of the above, we can add one more remark about the complete structure of the set of directions of \mathbf{B} , corresponding to the reconstructions of the structure of system (I.1). Namely, consider some structure of the system (I.1) on the Fermi surface containing a certain number of cylinders of closed trajectories. Then for each of the cylinders of closed trajectories it is possible to determine the region in the space of directions of \mathbf{B} (on the sphere \mathbb{S}^2) corresponding to the conservation of this cylinder (Fig. 41). The boundary of this region represents a (generally piecewise smooth) curve, at the intersection of which the selected cylinder disappears. The net of directions of \mathbf{B} we consider (including the boundaries of the Stability Zones) is the union of all the boundaries of the regions introduced in this way (for all different structures of (I.1) on the Fermi surface) intersecting with each other.

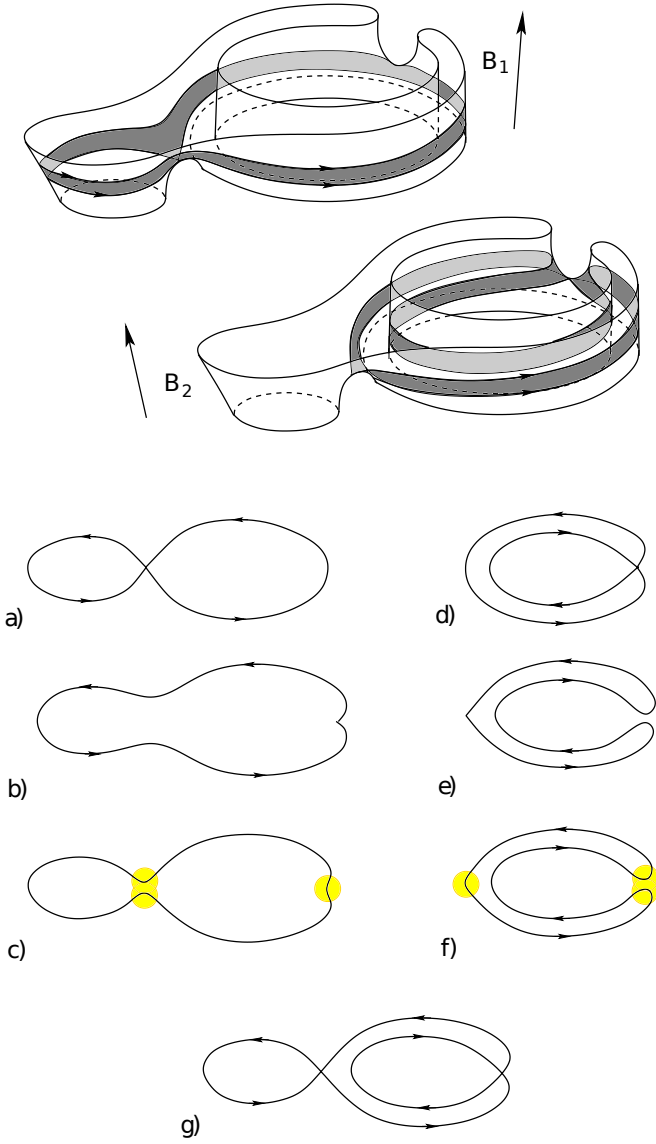


FIG. 31: A reconstruction of the structure of system (I.1) on a part of the Fermi surface. The lower and upper bases of the disappearing cylinder of closed trajectories and the extremal trajectory arising on it (a-c). The lower and upper bases of the appearing cylinder of closed trajectories and the extremal trajectory arising on it (d-f). The “cylinder of zero height” that appears at the moment of reconstruction (g).

V. ON THE CONNECTION OF THE DIAGRAM OF RECONSTRUCTIONS OF THE STRUCTURE OF (I.1) WITH THE GEOMETRY OF THE FERMION SURFACE.

Here we briefly describe how the picture of reconstructions of the structure of system (I.1) on the angular diagram and the observation of oscillation phenomena on special extremal trajectories can be used to reconstruct the geometry of the Fermi surface. As we have already said, the main feature of the special extremal trajectories

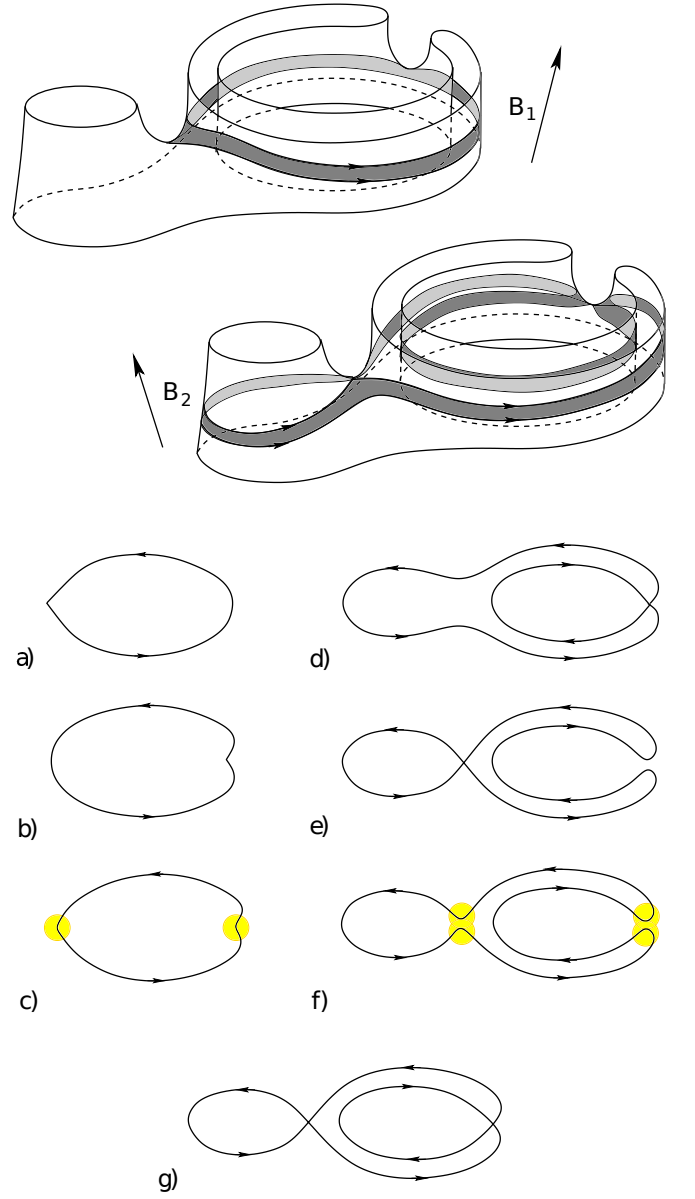


FIG. 32: A reconstruction of the structure of system (I.1) on a part of the Fermi surface. The lower and upper bases of the disappearing cylinder of closed trajectories and the extremal trajectory arising on it (a-c). The lower and upper bases of the appearing cylinder of closed trajectories and the extremal trajectory arising on it (d-f). The “cylinder of zero height” that appears at the moment of reconstruction (g).

is their very close approximation to singular trajectories for the directions of \mathbf{B} close to directions of the reconstruction of the structure of (I.1). The limit of each of the special extremal trajectories is a part (or the whole cylinder) of a “cylinder of zero height”, representing two singular points connected by singular trajectories. Let us connect the corresponding singular points of (I.1) with a vector (segment) $\xi_{\mathbf{p}}$ lying in the plane orthogonal to \mathbf{B} (see e.g. Fig. 42).

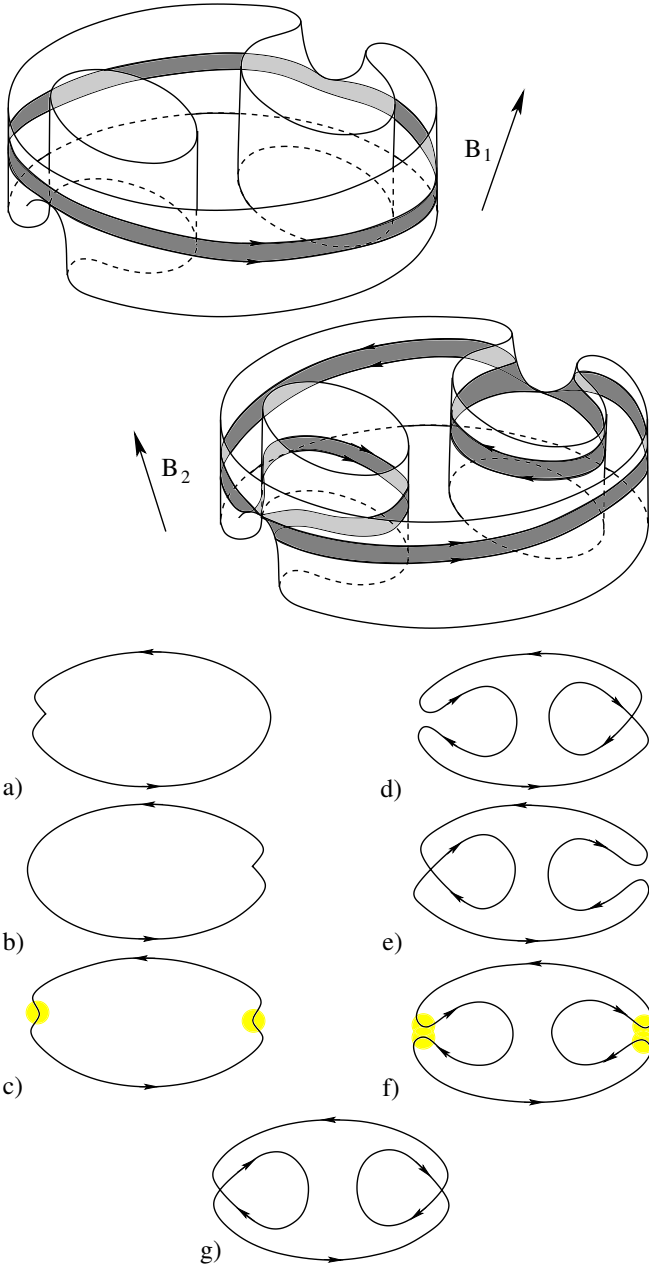


FIG. 33: A reconstruction of the structure of system (I.1) on a part of the Fermi surface. The lower and upper bases of the disappearing cylinder of closed trajectories and the extremal trajectory arising on it (a-c). The lower and upper bases of the appearing cylinder of closed trajectories and the extremal trajectory arising on it (d-f). The “cylinder of zero height” that appears at the moment of reconstruction (g).

As we saw above, the set of directions of \mathbf{B} , corresponding to reconstructions of the structure of system (I.1) on the Fermi surface, is in the general case a union (generally speaking, of an infinite number) of one-dimensional curves on the unit sphere. It is easy to see that small rotations of \mathbf{B} along the direction of $\xi_{\mathbf{p}}$ correspond to linear variations in the height of the

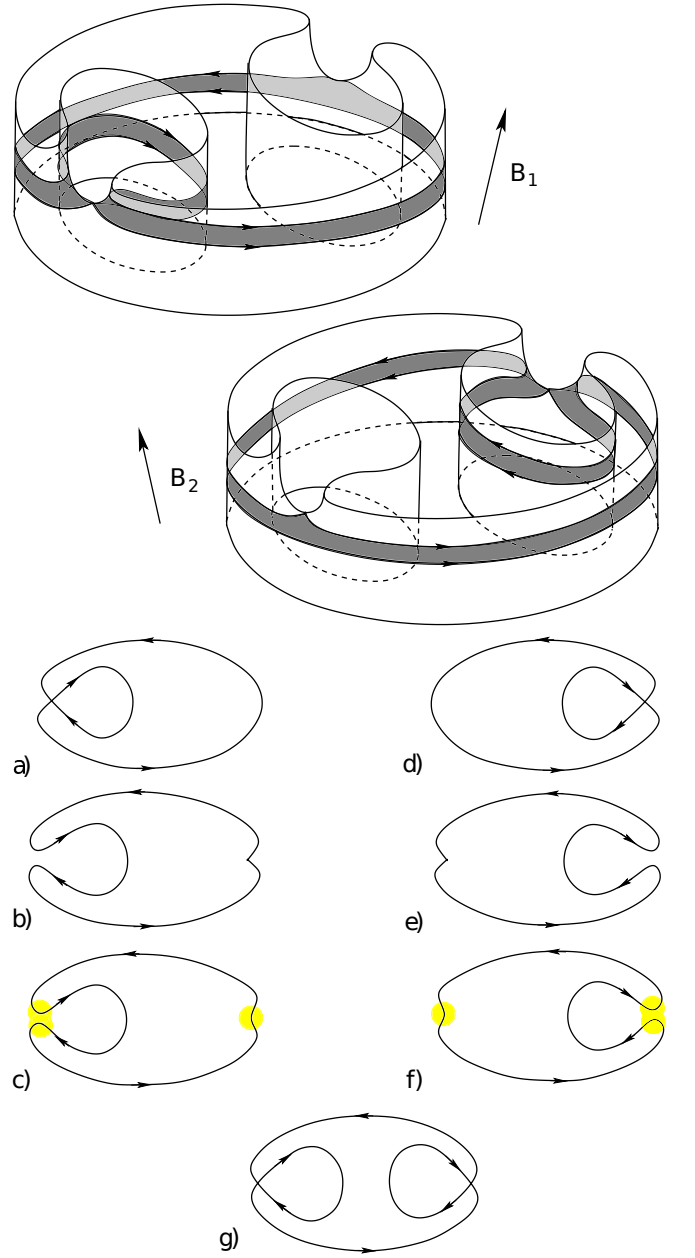


FIG. 34: A reconstruction of the structure of system (I.1) on a part of the Fermi surface. The lower and upper bases of the disappearing cylinder of closed trajectories and the extremal trajectory arising on it (a-c). The lower and upper bases of the appearing cylinder of closed trajectories and the extremal trajectory arising on it (d-f). The “cylinder of zero height” that appears at the moment of reconstruction (g).

corresponding cylinder of closed trajectories, while the rotations of \mathbf{B} in the direction orthogonal to $\xi_{\mathbf{p}}$ do not change the height of the cylinder in the linear approximation. One can see, therefore, that the tangent to the arc on \mathbb{S}^2 , corresponding to a reconstruction of the topological structure of (I.1), is always orthogonal to the corresponding vector $\xi_{\mathbf{p}}$ defined above. In other words, for

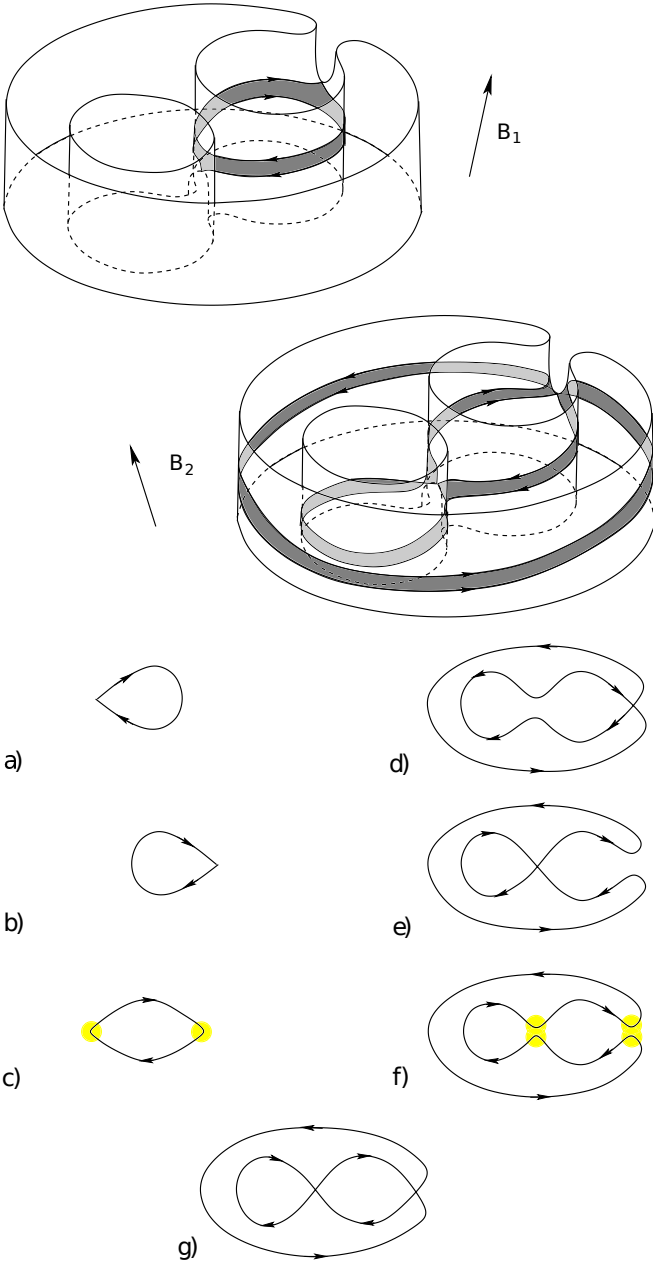


FIG. 35: A reconstruction of the structure of system (I.1) on a part of the Fermi surface. The lower and upper bases of the disappearing cylinder of closed trajectories and the extremal trajectory arising on it (a-c). The lower and upper bases of the appearing cylinder of closed trajectories and the extremal trajectory arising on it (d-f). The “cylinder of zero height” that appears at the moment of reconstruction (g).

a direction of \mathbf{B} lying on an arc γ , corresponding to the disappearance of a certain cylinder of closed trajectories on the Fermi surface, the corresponding vector $\xi_{\mathbf{p}}(\mathbf{p})$ in \mathbf{p} -space is parallel to the vector $\mathbf{B} \times \mathbf{s}(\mathbf{B})$, where $\mathbf{s}(\mathbf{B})$ is the tangent vector to the arc γ on \mathbb{S}^2 (Fig. 43).

When the direction of \mathbf{B} moves along the curve of the change of the structure of system (I.1), the beginning

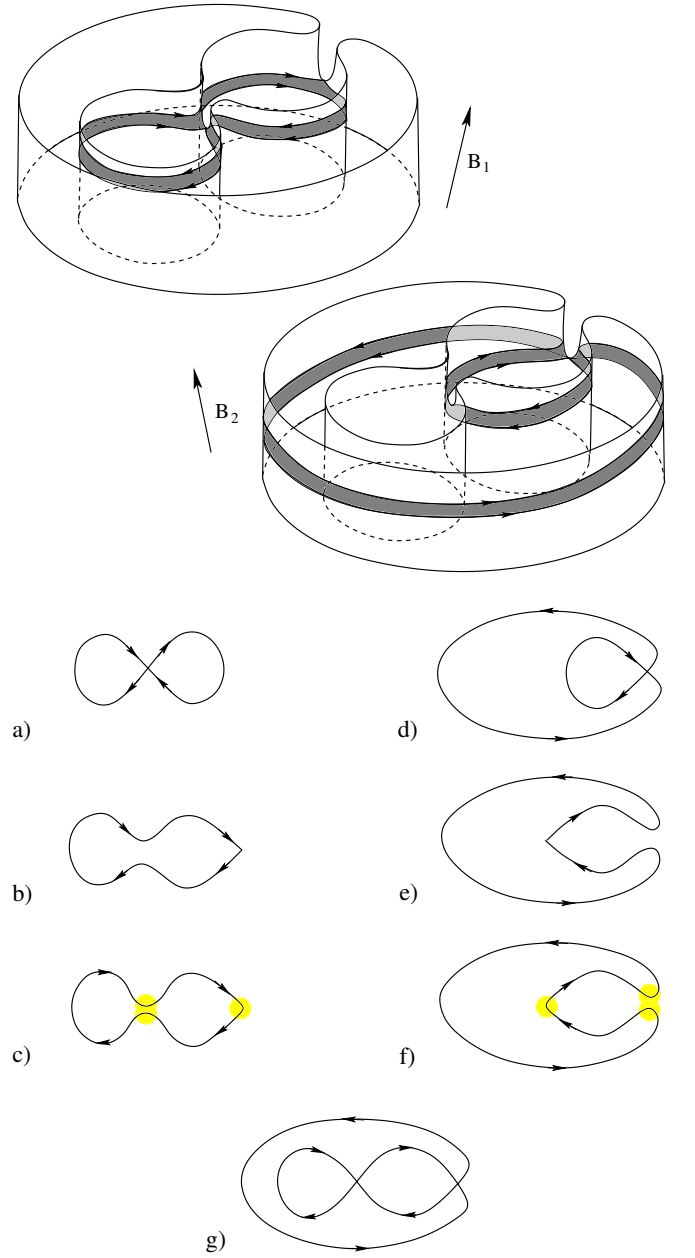


FIG. 36: A reconstruction of the structure of system (I.1) on a part of the Fermi surface. The lower and upper bases of the disappearing cylinder of closed trajectories and the extremal trajectory arising on it (a-c). The lower and upper bases of the appearing cylinder of closed trajectories and the extremal trajectory arising on it (d-f). The “cylinder of zero height” that appears at the moment of reconstruction (g).

and end of the vector $\xi_{\mathbf{p}}$ move along one-dimensional curves $\hat{\gamma}_{1,2}$ in the \mathbf{p} -space, and at each point of these curves the vector $\xi_{\mathbf{p}}$ is tangent to the Fermi surface. The direction of the normal to the Fermi surface (i.e., $\mathbf{v}_{gr}(\mathbf{p})$) coincides at these points with the corresponding direction

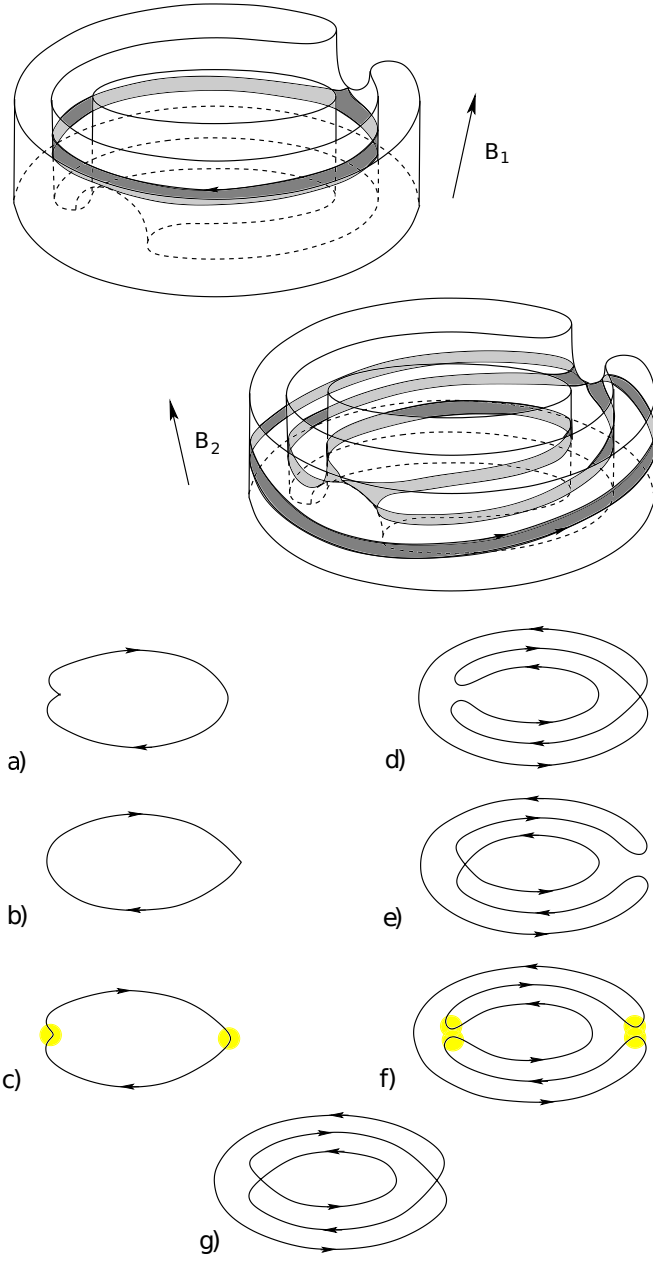


FIG. 37: A reconstruction of the structure of system (I.1) on a part of the Fermi surface. The lower and upper bases of the disappearing cylinder of closed trajectories and the extremal trajectory arising on it (a-c). The lower and upper bases of the appearing cylinder of closed trajectories and the extremal trajectory arising on it (d-f). The “cylinder of zero height” that appears at the moment of reconstruction (g).

of \mathbf{B} and we can also say that the Gauss map

$$S_F \rightarrow \mathbb{S}^2$$

maps the curves $\hat{\gamma}_1$ and $\hat{\gamma}_2$ to the curve γ and the diametrically opposite curve on \mathbb{S}^2 .

Unlike trajectories of the system (I.1), the curves $\hat{\gamma}_{1,2}$ are not, generally speaking, plane curves in the \mathbf{p} -space.

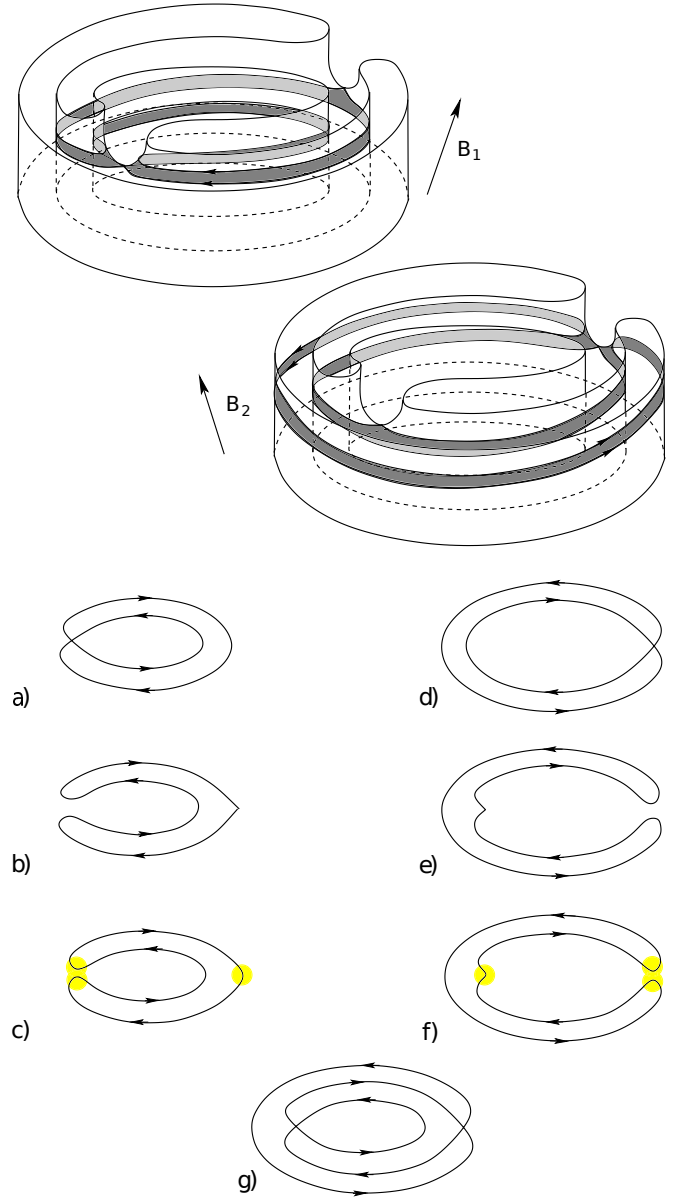


FIG. 38: A reconstruction of the structure of system (I.1) on a part of the Fermi surface. The lower and upper bases of the disappearing cylinder of closed trajectories and the extremal trajectory arising on it (a-c). The lower and upper bases of the appearing cylinder of closed trajectories and the extremal trajectory arising on it (d-f). The “cylinder of zero height” that appears at the moment of reconstruction (g).

If the “disappearing” cylinder of closed trajectories corresponding to the arc γ has central symmetry, then the center of the segment $\xi_{\mathbf{p}}$ remains motionless when the direction of \mathbf{B} moves along γ and coincides with one of the centers of symmetry of the Fermi surface in \mathbf{p} -space. We can see that in this case the exact knowledge of the shape of the curve γ (for example, the first or second boundary of a Stability Zone), as well as the length of the vector $\xi_{\mathbf{p}}$ for each of the points of γ , allows us to

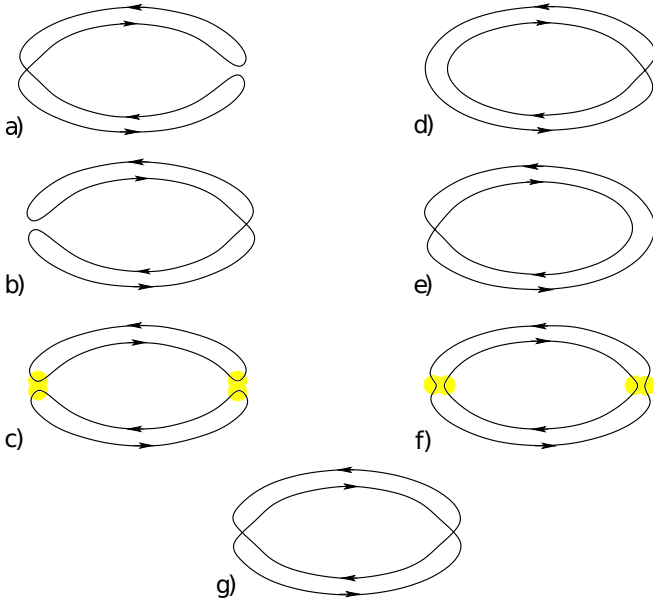
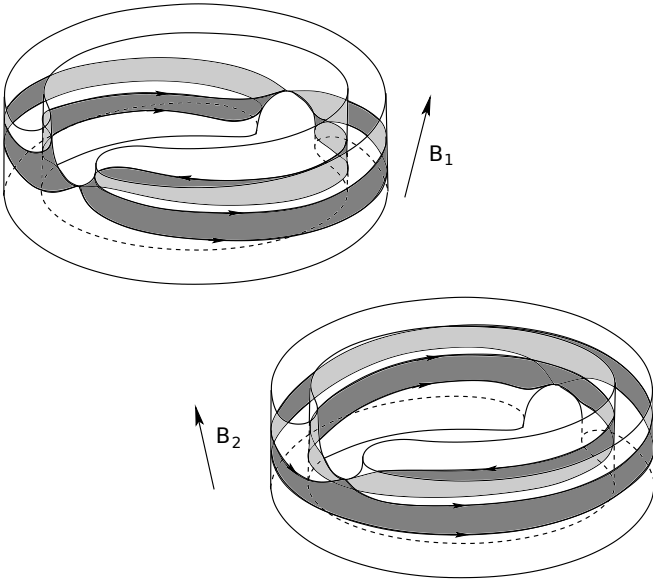


FIG. 39: A reconstruction of the structure of system (I.1) on a part of the Fermi surface. The lower and upper bases of a pair of disappearing cylinders of closed trajectories and a pair of extremal trajectories arising on them (a-c). The lower and upper bases of a pair of appearing cylinders of closed trajectories and a pair of extremal trajectories arising on them (d-f). The “cylinder of zero height” that appears at the moment of reconstruction (g).

restore two “infinitely narrow bands” on the Fermi surface corresponding to the movement of the end points of the segment $\xi_{\mathbf{p}}$ (Fig. 44). (We note here that the interior points of $\xi_{\mathbf{p}}$ can intersect the Fermi surface in this situation).

One can see, therefore, that on the arcs γ , corresponding to the disappearance of the centrally symmetric cylin-

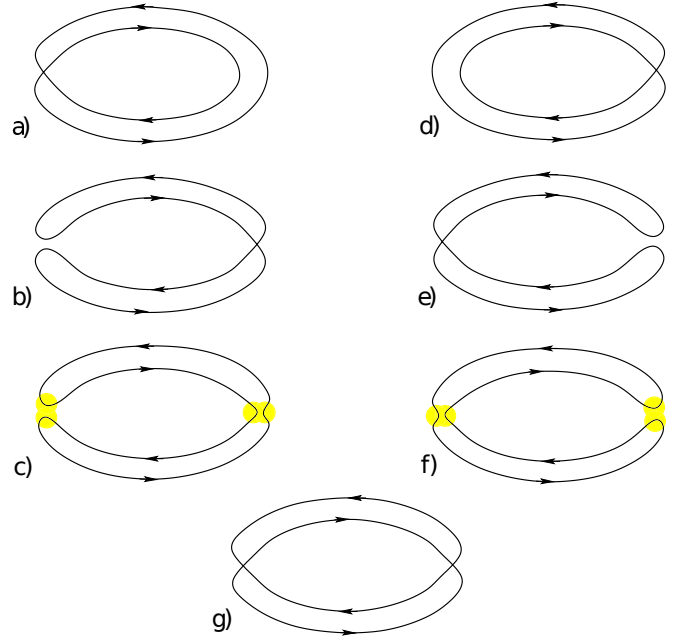
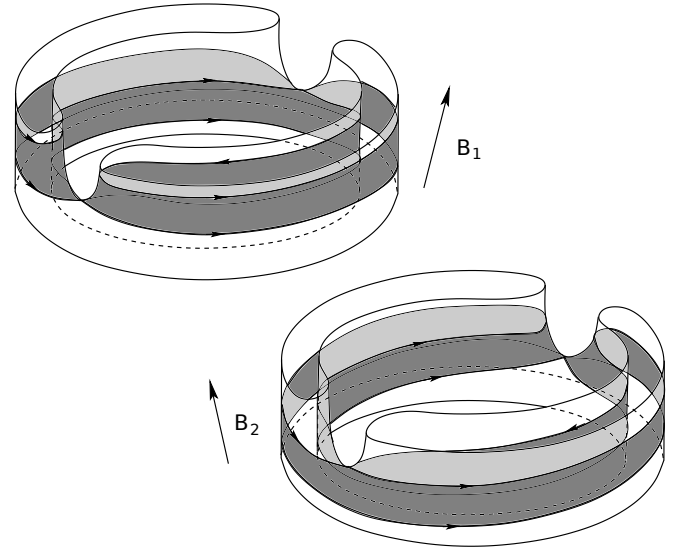


FIG. 40: A reconstruction of the structure of system (I.1) on a part of the Fermi surface. The lower and upper bases of the disappearing cylinder of closed trajectories and the extremal trajectory arising on it (a-c). The lower and upper bases of the appearing cylinder of closed trajectories and the extremal trajectory arising on it (d-f). The “cylinder of zero height” that appears at the moment of reconstruction (g).

ders of closed trajectories, we can indicate an effective procedure for reversing the Gauss map and restoring the inverse images $\hat{\gamma}_{1,2}$ on the Fermi surface along with the direction of the normal to S_F . As we could see above, for sufficiently complex Fermi surfaces, the sets of directions of \mathbf{B} , corresponding to reconstructions of the structure of system (I.1), form a fairly dense net at the angular diagram, which corresponds to an equally dense net of

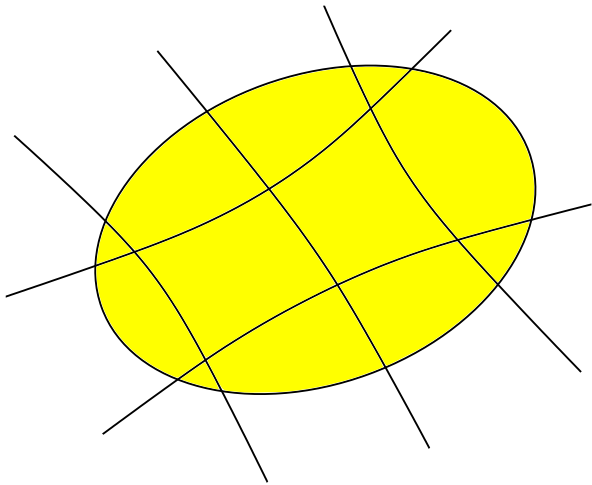


FIG. 41: The domain on the sphere \mathbb{S}^2 , corresponding to the existence of a certain cylinder of closed trajectories on the Fermi surface (schematically).

inverse images $\hat{\gamma}_{1,2}$ on the Fermi surface. The curves $\hat{\gamma}_{1,2}$ are formed by saddle singular points of the system (I.1) and, therefore, always lie on a part of the Fermi surface that has negative (Gaussian) curvature. It can be noted here that, with a more general consideration, the methods for reconstructing the Fermi surface, based on the study of the presented special extremal trajectories, are connected, first of all, with that part of the Fermi surface where it has negative Gaussian curvature.

In a more general situation, when the experimental design does not imply a separate measurement of the length of the vector $\xi_{\mathbf{p}}$, each curve γ , corresponding to the disappearance of a centrally symmetric cylinder of closed trajectories, gives us a (one-parameter) family of lines passing through a given center of symmetry and tangent to the Fermi surface. Each such family provides important information about the Fermi surface (its part having negative curvature), which is also convenient to use to refine its shape.

In considering the formation and disappearance of centrally symmetric cylinders of closed trajectories, we must, of course, discuss also the following question. Considering centers of symmetry of a periodic dispersion relation $\epsilon(\mathbf{p})$, we can immediately say that there are always actually several such symmetry centers (nonequivalent to each other) in the \mathbf{p} -space. It is easy to see that in the most general case it is possible to choose the Brillouin zone (parallelepiped in \mathbf{p} -space) so that such centers are: the center of the parallelepiped, the centers of its faces, the centers of its edges and its vertices (Fig. 45).

The centers of the opposite faces of the parallelepiped are pairwise equivalent to each other, the centers of the edges form 3 fours of equivalent centers, and all the vertices of the parallelepiped represent one center after factorization by the reciprocal lattice vectors. Thus, in the general case, we always have 8 nonequivalent centers of

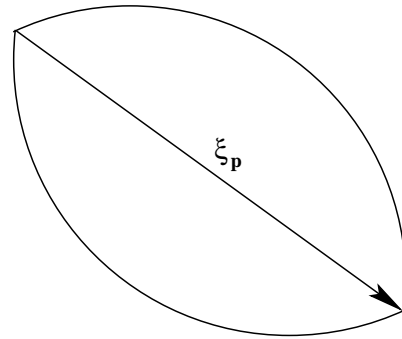
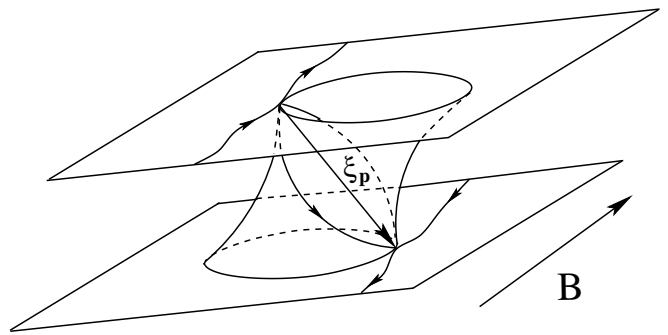


FIG. 42: The vector $\xi_{\mathbf{p}}$ connecting two singular points on a special singular trajectory in the \mathbf{p} -space.

symmetry in the \mathbf{p} -space. In other words, we have 8 nonequivalent periodic families of centers of symmetry that transform into each other when shifted by half-integer reciprocal lattice vectors.

The presence of the central symmetry in a cylinder of closed trajectories means that when reflected with respect to any of the centers of symmetry, such a cylinder transforms into an equivalent cylinder (shifted by a reciprocal lattice vector) in \mathbf{p} -space. For each such cylinder there is a unique point in \mathbf{p} -space, the reflection with respect to which takes the cylinder into itself. It is easy to see that for the construction of the curves $\hat{\gamma}_{1,2}$ described above, we need, among other things, to know which of the periodic families of centers of symmetry this point belongs to.

It can also be seen that the correspondence between the centrally symmetric cylinders of closed trajectories and their “own” centers of symmetry in the \mathbf{p} -space remains unchanged until any of these cylinders disappears and, therefore, also applies to the definition of the topological structure of the system (I.1) on the Fermi surface. In addition, for any elementary reconstruction of the structure of (I.1), the disappearance of one centrally symmetric cylinder of closed trajectories also leads to the appearance of a centrally symmetric cylinder of closed trajectories with the same “own” center of symmetry (also coinciding with the “own” center of symmetry

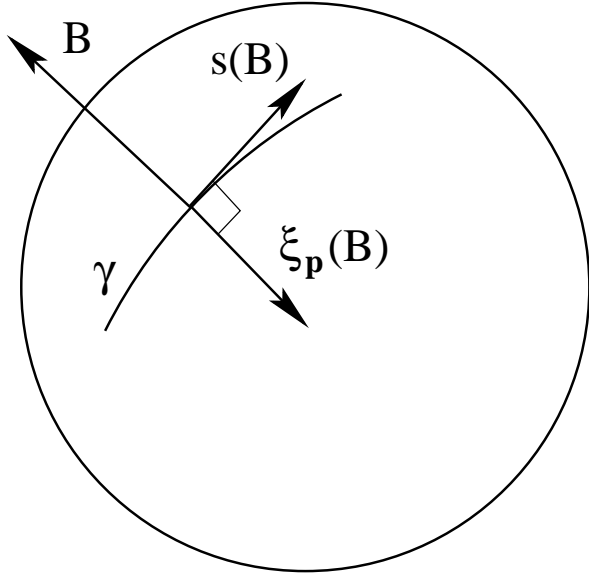


FIG. 43: The direction of the vector $\xi_{\mathbf{p}}$ corresponding to a given direction of \mathbf{B} on a curve of the change of the structure of system (I.1) on the Fermi surface.

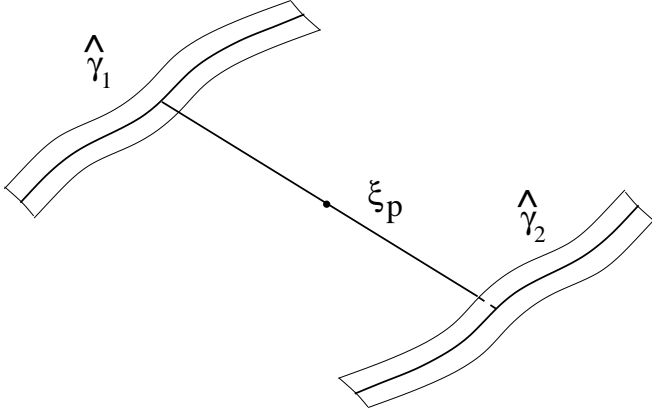


FIG. 44: Two infinitely narrow bands on the Fermi surface defined by the movement of the ends of the segment $\xi_{\mathbf{p}}$ when the direction of \mathbf{B} rotates along a curve of the change of the structure of system (I.1).

of the corresponding “cylinder of zero height”). In particular, we can see that if for two directions of \mathbf{B} :

1) it is possible to move from one direction to another with a finite number of elementary reconstructions of the structure of (I.1);

2) each of the appearing “cylinders of zero height” during the motion corresponds to the appearance and disappearance of only one cylinder of closed trajectories;

then the structure of the system (I.1) for such directions contains the same number of centrally symmetric cylinders of closed trajectories with the same “own” cen-

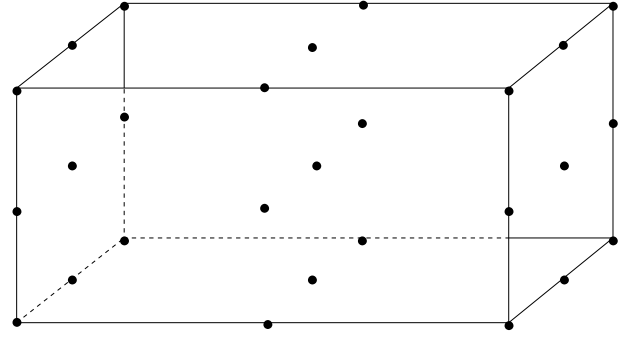


FIG. 45: Brillouin zone and symmetry centers of a dispersion relation $\epsilon(\mathbf{p})$ in \mathbf{p} - space.

ters of symmetry.

Thus, under the above conditions, connecting two directions \mathbf{B}_1 and \mathbf{B}_2 by a suitable curve at the angular diagram, we can establish a correspondence between the centrally symmetric cylinders of closed trajectories that occur for both directions, matching the disappearing cylinder the one that appears during each reconstruction. In particular, in such a correspondence, we can indicate, for example, the “own” symmetry centers of such cylinders for the direction \mathbf{B}_2 , if they were known for the direction \mathbf{B}_1 .

This circumstance may be convenient in the experimental study of reconstructions of the structure of system (I.1), since it allows one to obtain additional data on cylinders of closed trajectories for the directions of \mathbf{B} , for which an independent study of the structure of (I.1) can be difficult. In particular, if approximate information about the Fermi surface geometry is sufficient to determine the topological structure of system (I.1) for the direction \mathbf{B}_1 , then by observing the reconstructions along the path connecting \mathbf{B}_1 and \mathbf{B}_2 , we can also obtain the necessary data for the direction \mathbf{B}_2 , where such information is not sufficient. This situation is actually quite general, thus, the first case usually occurs in those areas of the angle diagram where the net of directions of \mathbf{B} corresponding to the reconstructions of the structure of (I.1) is not dense, and the second - in areas where such a net is very dense. In this case, each of the cylinders of closed trajectories can be associated with the corresponding contribution in the overall picture of oscillations, and we can continue this matching from the direction \mathbf{B}_1 to \mathbf{B}_2 , associating in reconstructions the arising cylinder with a new oscillation term. This matching allows, in particular, to indicate the “own” center of symmetry of a centrally symmetric cylinder corresponding to any oscillation term observed at the direction \mathbf{B}_2 .

We note again that we represent the general picture of oscillations when observing oscillations of various types as the sum of a finite number of oscillating terms corresponding to extremal trajectories on the Fermi surface. As we noted above, the main feature in the behavior of

such oscillations for us is a sharp change in the overall picture with a change in the topological structure of (I.1), which allows us to observe the net of directions of \mathbf{B} on \mathbb{S}^2 , corresponding to changes in this structure. More precisely, as we have already said, a change in the oscillation picture during each “elementary” reconstruction of the system (I.1) consists in the disappearance of one of the oscillation terms in the total sum of oscillations and its replacement by another one (or simply the disappearance of one of the oscillation terms at the boundary of a Stability Zone).

It can be noted here again that, as we have already said, reconstructions containing “cylinders of zero height” corresponding to the disappearance and appearance of pairs of cylinders of closed trajectories can appear only in special cases on rather complex Fermi surfaces. For a large class of real Fermi surfaces, the above conditions will actually be satisfied for any two directions of \mathbf{B} , which can be connected by a path that does not intersect the boundaries of the Stability Zones or segments of the appearance of periodic trajectories.

Coming back to the reconstructions corresponding to the disappearance and appearance of cylinders of closed trajectories that do not have central symmetry, we can immediately note that the number of such reconstructions at the angular diagram is rather small even for fairly complex Fermi surfaces. The determination of the shape of the corresponding curve γ at the angular diagram also determines here the direction of the vector $\xi_{\mathbf{p}}(\mathbf{B})$ connecting two saddle singular points of the system (I.1). In the \mathbf{p} -space we have now two non-equivalent segments with the common direction $\xi_{\mathbf{p}}(\mathbf{B})$, each of which is tangent to the Fermi surface at two points. Thus, in this case, we can say that we have a segment of a given direction which is tangent to the Fermi surface at two points that do not pass into each other upon reflection (and also a segment symmetrical to it). Such data on the Fermi surface look somewhat more complicated in comparison with the centrally symmetric case, however, we can verify that they have the same information content from the functional point of view.

We can still make a small remark regarding the reconstructions, in which the disappearance (and appearance) of a pair of cylinders of closed trajectories occurs (Fig. 39). If the Fermi surface is not ultra-complex, it is natural to assume that in such reconstruction we observe a disappearance of a pair of cylinders with central symmetry, and the appearance of a pair of cylinders that pass into each other under the central reflection. From the experimental point of view, this reconstruction differs from the others by the disappearance of two oscillation terms in the total picture of oscillations and their replacement by one term (in fact, two coinciding ones coming from a pair of extremal trajectories that are symmetrical to each other). In this situation, as in the case of the disappearance of a single centrally symmetric cylinder, the segment $\xi(\mathbf{B})$ is unique and passes through one of the symmetry centers in the \mathbf{p} -space. The corresponding

center of symmetry coincides with the “own” center of symmetry of the disappearing cylinders and the refinement of the geometry of the Fermi surface can be carried out in the same way as in the case of the disappearance of one centrally symmetric cylinder.

Let us consider at the end of this chapter some aspects of observing the cyclotron resonance phenomenon on the special extremal trajectories, related to the peculiarities of their geometry.

As is well known, electron trajectories in the \mathbf{x} -space have geometric properties that are somewhat similar to the geometric properties of the trajectories of the system (I.1) in the quasimomenta space. In particular, the projections of the trajectories in the \mathbf{x} -space onto the plane orthogonal to \mathbf{B} are similar to the trajectories in the \mathbf{p} -space rotated by 90° . The similarity coefficient between the trajectories in the momentum space and their projections onto the plane orthogonal to \mathbf{B} in the coordinate space is equal to c/eB . In general, all the trajectories in the \mathbf{x} -space decrease in size with the growth of B , like B^{-1} , without changing their geometric shape.

It is easy to see that the special trajectories we consider correspond in the \mathbf{x} -space to either closed trajectories (in the presence of central symmetry) or spiral trajectories of a special shape (in the absence of central symmetry) that describe a constant drift along the magnetic field (see e.g. Fig. 46). In both cases, one can note the presence of almost vertical (parallel to \mathbf{B}) sections due to the presence of sections in \mathbf{p} -space, close to singular points of the system (I.1), at which the group velocity is almost parallel to \mathbf{B} and the speed of motion along the trajectory is very small. Here we will consider the observation of cyclotron resonance at \mathbf{B} , parallel to the surface of the sample, so we can see that when such areas get into the skin layer (Fig. 55), the electrons can spend quite a lot of time in the skin layer, while moving mainly along the direction of \mathbf{B} . One can immediately note, therefore, that the amplitude of the absorption oscillations in the cyclotron resonance should in this situation be maximal when the electric field in the incident wave \mathbf{E}_w is parallel to \mathbf{B} . This, in particular, can serve as one of the signs that distinguishes the situation under consideration from the general one (getting into the skin layer of an arbitrary part of the trajectory), when the maximal absorption is observed when $\mathbf{E}_w \parallel \mathbf{v}_{gr}$, where the direction of \mathbf{v}_{gr} at the section falling into the skin layer is different from the direction of \mathbf{B} .

The situation where the “deceleration region” gets into the skin layer can be typical, for example, when measuring $|\xi_{\mathbf{x}}|$ (and with it $|\xi_{\mathbf{p}}|$) by cutting off cyclotron orbits (see [47]) or by a non-resonant size effect ([48]) for the most common special extremal trajectories (Fig. 47). We note here that such a method of measuring of $|\xi_{\mathbf{p}}|$ is perhaps the most convenient, since, as we have already said, the direction of $\xi_{\mathbf{x}}$ relative to the crystal lattice is known for any point on the curve of the reconstruction of the structure of (I.1), so that the thickness of the film on which the extremal orbits are cut off can easily be

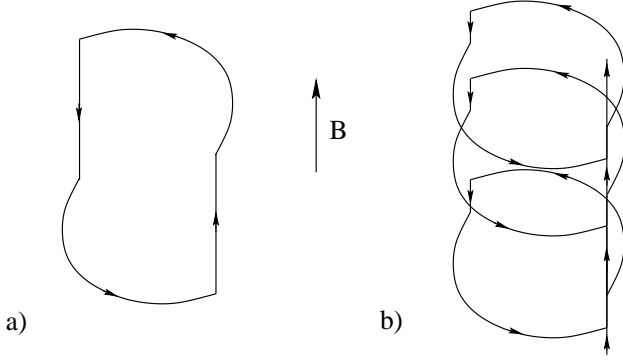


FIG. 46: Trajectories in \mathbf{x} - space corresponding to special extremal trajectories of the system (I.1) in the presence (a) and absence (b) of central symmetry.

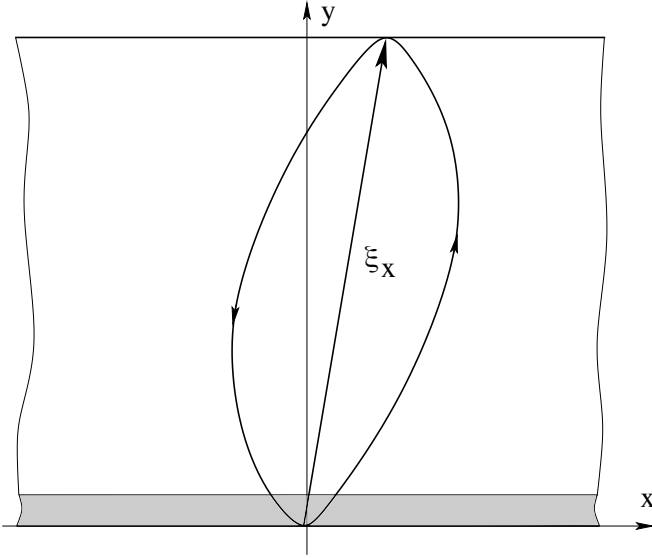


FIG. 47: Measuring of $|\xi_x|$ by cutting off cyclotron orbits for a special extremal trajectory of the most common geometry.

correlated with the value of $|\xi_x|$.

It can be noted here that the “deceleration regions” on the trajectories in \mathbf{p} - space can also manifest themselves in the case when an “ordinary” trajectory segment gets into the skin layer in a cyclotron resonance situation. Namely, such sections can create narrow current layers inside the sample with the direction of the current along the magnetic field. Such current layers should arise together with the layers corresponding to the points of the trajectory at which the group velocity is parallel to the sample boundary, differing from them in the direction and amplitude of the arising currents. Each special extremal trajectory gives rise to two different current layers of the first type, corresponding to two saddle singu-

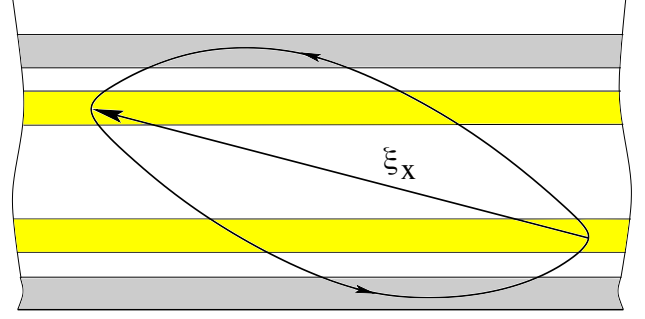


FIG. 48: Current layers of the first and second type generated by special extremal trajectories inside the sample.

lar points present on the corresponding “cylinder of zero height”. Like the layers of the second type, the layers corresponding to the “deceleration regions” are parallel to the boundary of the sample (Fig. 48). The distance between two layers generated by two different “deceleration regions”, as is easily seen, is equal to the length of projection of the vector ξ_x on the normal to the sample boundary.

It should also be noted here, in addition, that among the types of special extremal trajectories given in the previous chapter, only a part allows the deceleration section to enter the skin layer at the sample boundary, which is due to the local geometry of such trajectories near special points on the corresponding “zero-height cylinder”. Let us list these types here.

We begin here with the most basic type, corresponding to the trajectory arising at the reconstruction shown at Fig. 25 - 26 (Fig. 49). Trajectories of the same type also arise during the reconstruction shown at Fig. 12, the reconstruction shown at Fig. 35 (trajectory (c)), the reconstruction shown at Fig. 39 (one of the trajectories (f)), as well as near the boundaries of the Stability Zones Ω_α . As for the reconstruction shown at Fig. 25 - 26, and for the reconstructions shown at Fig. 12, 35, and Fig. 39, such trajectories occur only on one side from the line of reconstruction of the structure of (I.1) (as well as only on the inner side of a Stability Zone boundary). It is easy to see that any of the “deceleration sections” on the presented trajectory can enter the skin layer at a suitable orientation of the crystal lattice of the sample. Group velocities in two “deceleration regions” on such trajectories are directed opposite to each other and, as we have already said, in the overwhelming majority of cases, trajectories of this type possess central symmetry. In rare cases, however, such trajectories can also occur in pairs, turning into each other under the transformation of central symmetry. In the latter case, group velocities at different “deceleration sections” can differ from each other in absolute value.

Let us make one more remark here. Namely, the trajectory shown at Fig. 49 has, in fact, to some extent an ideal

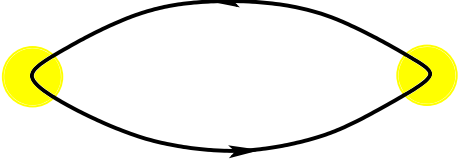


FIG. 49: A special extremal trajectory of the most common type.

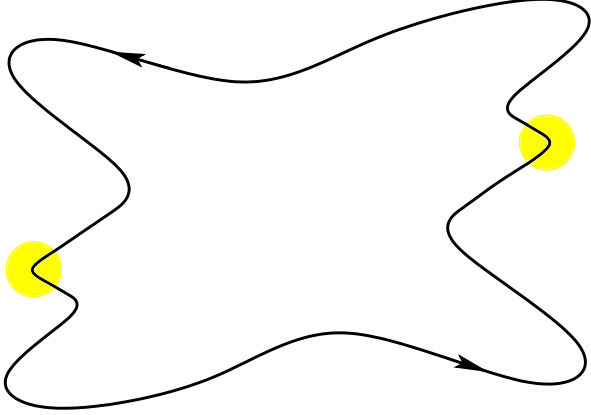


FIG. 50: A special extremal trajectory of complex shape that does not allow the “deceleration sections” to enter the skin layer.

shape and can be significantly more complex geometrically in some cases. In particular, despite the consistency of the required situation (the “deceleration section” in the skin layer) with the local trajectory geometry, this situation can still be prohibited by the global properties of the trajectory (see for example, Fig. 50). It should be said that in such cases the shape of such a trajectory changes quite quickly when the direction of \mathbf{B} moves along the corresponding curve of the reconstruction of the structure of system (I.1) at the angular diagram. The situation we require then, as a rule, becomes possible not on the entire curve γ , but only on certain sections of it. We also note that the remark made will equally apply to the other types of trajectories considered below.

The second type of special extremal trajectories that allow the “deceleration section” to enter the skin layer can include trajectories of similar shape, shown at Fig. 32(c) and 37(c) (Fig. 51). In both cases, trajectories of this shape arise only on one side of the corresponding reconstruction curve γ at the angular diagram. Both cases, presented at Fig. 32 and 37, do not have central symmetry, therefore, the corresponding reconstructions can arise only in pairs and, in particular, each of the trajectories shown at Fig. 32 (c) and 37 (c) always arise in pair with a trajectory symmetric to it (located on a part

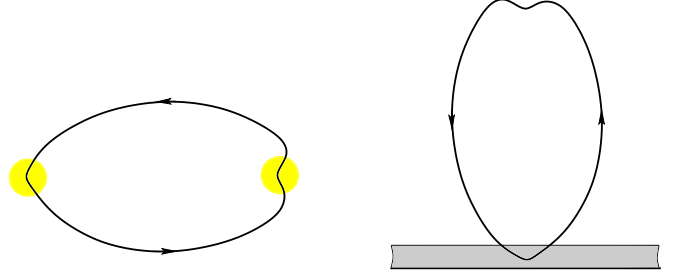


FIG. 51: A special extremal trajectory of the second type, allowing the “deceleration section” to enter the skin layer.

of the Fermi surface symmetric to the one under consideration). However, there is also a significant difference between the trajectories shown at Fig. 32 (c) and 37 (c). Namely, for the trajectory shown at Fig. 32 (c) the group velocities $\mathbf{v}_{gr}(\mathbf{p})$ at the two “deceleration sections” are co-directional, while for the trajectory, shown at Fig. 37 (c), they are directed opposite to each other. The latter circumstance, as is easily seen, should play a significant role in considering the penetration of the “current layers” (parallel to the boundary of the sample) into the sample in our situation.

The third type of special extremal trajectories that allow the “deceleration section” to enter the skin layer can be trajectories of similar shape, shown at Fig. 31 (f) and 38 (c) (Fig. 52). As in the previous case, in both cases trajectories of this shape arise only on one side of the corresponding reconstruction curve γ at the angular diagram. Both cases, presented at Fig. 31 and 38, do not have central symmetry, so the corresponding reconstructions can occur only in pairs and, in particular, each of the trajectories shown at Fig. 31 (f) and 38 (c) always arise in pair with a trajectory symmetrical to it. Between the trajectories shown at Fig. 31 (f) and 38 (c), as in the previous case, there is a difference in the direction of the group velocity at the “deceleration sections”. Thus, for the trajectory shown at Fig. 31 (f), the group velocity at the “deceleration section” falling into the skin layer is opposite in direction to the group velocity at the other two “deceleration sections”, while for the trajectory, shown at Fig. 38 (c), group velocities at all “deceleration sections” are co-directed.

The next type of special extremal trajectories that allow the “deceleration section” to fall into the skin layer can be the trajectories shown at Fig. 28 (c,f) and 36 (c) (Fig. 53). In the case of the reconstruction shown at Fig. 27, trajectories of this form arise on both sides of the curve of reconstruction of the structure of (I.1). In this case, however, the trajectories on one side of the reconstruction curve, generally speaking, are not identical to the trajectories on the other side of the reconstruction curve, therefore, the parameters of the corresponding oscillating terms change during the reconstruction of the

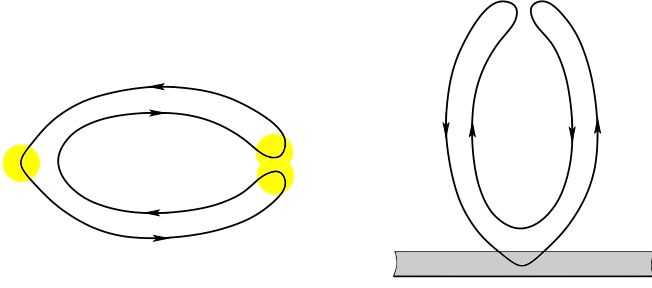


FIG. 52: A special extremal trajectory of the third type, allowing the “deceleration section” to enter the skin layer.

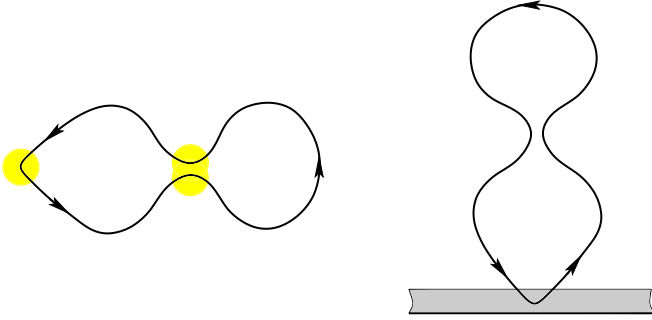


FIG. 53: A special extremal trajectory of the fourth type, allowing the “deceleration section” to enter the skin layer.

structure of (I.1). For the reconstruction, shown at Fig. 36 (c), trajectories of this shape arise only on one side of the corresponding reconstruction curve γ on the angular diagram. Both cases, presented at Fig. 27 and 36, do not have central symmetry, so the corresponding reconstructions can occur only in pairs and, in particular, each of the trajectories shown at Fig. 28 (c,f) and 36 (c) always appears in pair with a symmetrical trajectory to it. For all the presented trajectories, the group velocities are co-directional to each other at all three “deceleration sections” on the trajectory.

Finally, the last type of special extremal trajectories that allow the “deceleration sections” to enter the skin layer can be attributed to the trajectories shown at Fig. 39 (c) (Fig. 54). In the case of the reconstruction shown at Fig. 39, trajectories of this shape arise only on one side of the corresponding reconstruction curve γ on the angular diagram. The case presented at Fig. 39 has central symmetry and can occur on a single part of the Fermi surface. The two trajectories shown at Fig. 39 (c), are not connected to each other in the coordinate space and appear independently of each other. The main feature of the trajectories shown at Fig. 39(c) is that it is possible for them to place two “deceleration sections” at once into the skin layer at the sample boundary. Observation of cyclotron resonance in such a situation is, of course,

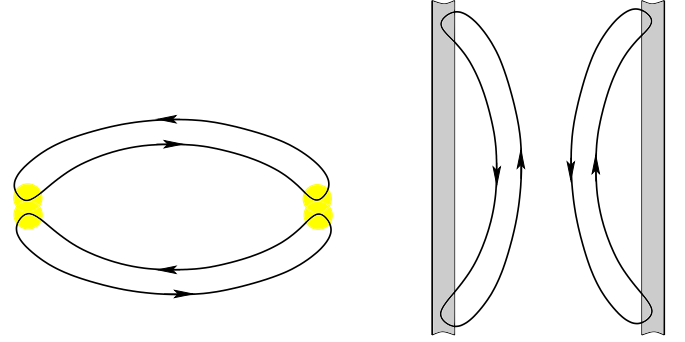


FIG. 54: A special extremal trajectory of the fifth type, allowing two “deceleration sections” to enter the skin layer at the boundary of the sample.

more complicated due to interference from the contributions originating from two boundary points. On each of the trajectories presented at Fig. 39 (c), the group velocities at the two “deceleration sections” are opposite to each other.

As it is easy to see, except the trajectories shown above, the other special extremal trajectories presented at Fig. 26, 28, 31 - 40 do not allow “deceleration sections” to fall into the skin layer due to the features of their local geometry near these sections.

VI. SOME FEATURES OF THE OBSERVATION OF OSCILLATION PHENOMENA ON SPECIAL EXTREMAL TRAJECTORIES.

This chapter is, to some extent, technical and is devoted to the peculiarities of observing of oscillation phenomena on the extremal trajectories described above. Most of it will actually be devoted to considering the features of observing cyclotron resonance when a “deceleration section” enters the skin layer near the surface of the sample. Besides that, we will consider some general features and limitations of observing the oscillation phenomena at very small angles of deviation of the direction of \mathbf{B} from the boundaries of the reconstruction of the structure of system (I.1).

We note here that different effects of the “deceleration sections” on semiclassical trajectories on the oscillation phenomena and, in particular, on the cyclotron resonance phenomenon, were considered, of course, earlier from different points of view. Let us also note that the deceleration sections on the trajectories can arise not only due to the presence of singular points of system (I.1) on the Fermi surface, but also due to the presence of a reconstruction of the constant-energy surface (Van Hoff singularity) near the Fermi level (see e.g. [49]). It can be noted here that the main difference between the two described situations consists, apparently, in preserving the

finite value of the component of \mathbf{v}_{gr} along the direction of \mathbf{B} in the first case and the proximity to zero of all components of \mathbf{v}_{gr} in the second.

From the most general conditions, we note, first of all, that all the phenomena considered by us can occur only at rather big mean free path of an electron in a crystal. In the purest single-crystal samples at low temperatures, the mean free time of electrons reaches $10^{-9} - 10^{-8} c$, and the corresponding mean free path $l \simeq 10^{-1} cm$. The value of the skin layer depth δ for the incident wave frequency $\nu \simeq 10^{10} Hz$, which is typical in a situation of cyclotron resonance observation, can be estimated in order of magnitude as $10^{-5} - 10^{-4} cm$. In our situation, the resonant frequencies can, in fact, be lower than the value of ν given here, since the period of circulation along special extremal trajectories can be longer than the period of circulation along “ordinary” closed trajectories. The value of δ , however, is rather weakly dependent on the frequency in the situation of anomalous skin effect ($\delta \sim \nu^{-1/3}$), therefore we will also use here the estimate $\delta \simeq 10^{-5} - 10^{-4} cm$. The size of a special extremal trajectory in the \mathbf{x} -space (its projection onto the plane orthogonal to \mathbf{B}) depends on the value of B . For the values $B \simeq 1 Tl$ for electrons in different metals we can take the estimate $r_B \simeq 10^{-3} - 10^{-2} cm$ and $r_B \simeq 10^{-4} - 10^{-3} cm$ for $B \simeq 10 Tl$.

As we have already said, we will be particularly interested in the case where the “deceleration section” on a special extremal trajectory falls into the skin layer at the boundary of the sample. For simplicity, we will assume here that the extremal trajectories have the most common centrally symmetric shape, shown at Fig. 49.

As is well known ([50, 51]), the main role in the phenomenon of classical cyclotron resonance is played by the accumulation of energy by electrons in the skin layer and the synchronization of the incident radiation frequency with an integer multiple of the frequency of the electron circulation along extremal closed trajectories on the Fermi surface. As a rule, it is assumed that electron spends a rather small part of the time in the skin layer and manages to return to the skin layer many times between two scattering acts. In a standard situation, the fraction of time spent by an electron in the skin layer can be estimated as $\sqrt{\delta/r_B}$, where δ is the depth of the skin layer, and the number of electron returns to the skin layer varies from several tens to several hundred. It is usually assumed that the phase of the incident wave remains almost unchanged during the time spent by electron in the skin layer for relatively small n in the relation $\Omega = n\omega_B$, where Ω is the frequency of the incident radiation. In the purest samples, cyclotron resonance can be observed up to rather large values of n , reaching several tens.

It can be seen that the conditions of observing the cyclotron resonance when a “deceleration section” enters the skin layer can, in fact, differ from the above. We should therefore consider the corresponding situation in more detail here.

For our purposes, we will need to reproduce the (stan-

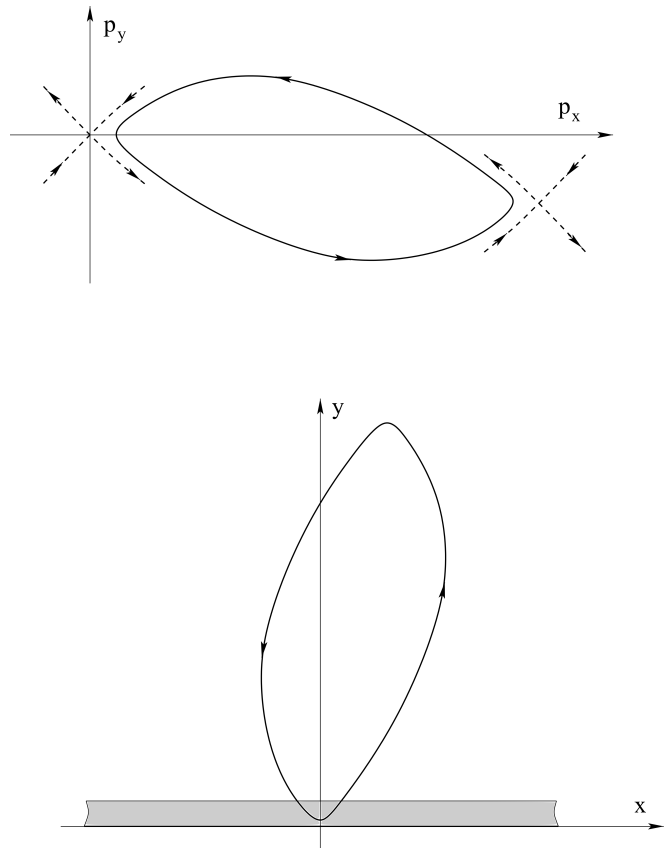


FIG. 55: Extremal trajectory in \mathbf{p} -space and the corresponding trajectory in \mathbf{x} -space passing through the skin layer at the surface of the sample (projection onto the plane orthogonal to \mathbf{B}).

dard) consideration of the shape of special extremal trajectories and the motion along them at the “deceleration sections”.

In our considerations, we will always assume that the axis z is directed along the magnetic field. In addition, we choose the axes x and y parallel to the directions of the principle curvatures at the currently considered saddle singular point close to the special trajectory on the “disappearing” cylinder of closed trajectories. For simplicity, we will also assume here that the boundary of the sample coincides with the plane xz (Fig. 55).

In general, the shape of a trajectory near a critical point in the \mathbf{p} -space is given by the equation

$$\frac{1}{2} \left(K_1 (\Delta p_x)^2 - K_2 (\Delta p_y)^2 \right) = \Delta p_z, \quad (\text{VI.1})$$

where K_1 and K_2 are the values of the principal curvatures of the Fermi surface at the critical point. The value of Δp_z is directly related to the angle of deviation of \mathbf{B} from the boundary of the reconstruction of the structure of system (I.1), since

$$\Delta p_z = \alpha |\xi_{\mathbf{p}}|/2 \quad (0 < \alpha \ll 1)$$

Thus, we can write

$$K_1 (\Delta p_x)^2 - K_2 (\Delta p_y)^2 = \alpha |\xi_{\mathbf{p}}| \quad (\text{VI.2})$$

In coordinate space directly from the equation (VI.2) follows the equation

$$K_1 (\Delta y)^2 - K_2 (\Delta x)^2 = \frac{c^2}{e^2 B^2} \alpha |\xi_{\mathbf{p}}| = \frac{c}{eB} \alpha |\xi_{\mathbf{x}}|$$

for the projection of a special extremal trajectory onto the plane orthogonal to \mathbf{B} . In particular, for $\Delta x = 0$ we get

$$\Delta y = \frac{c}{eB} \sqrt{\frac{\alpha |\xi_{\mathbf{p}}|}{K_1}}$$

for the distance from the trajectory to the intersection point of the asymptotes of the hyperbola.

By entering the notation $r_B = cp_F/eB$, the conditions $\Delta y \leq \delta$ and $\Delta y \geq \delta$ can be written as

$$\frac{1}{p_F} \sqrt{\frac{\alpha |\xi_{\mathbf{p}}|}{K_1}} \leq \frac{\delta}{r_B} \quad \text{and} \quad \frac{1}{p_F} \sqrt{\frac{\alpha |\xi_{\mathbf{p}}|}{K_1}} \geq \frac{\delta}{r_B}$$

Assuming approximately $|\xi_{\mathbf{p}}| \simeq p_F$ and $K_1 \simeq p_F^{-1}$, the above conditions can also be written as

$$\sqrt{\alpha} \leq \delta/r_B \quad \text{and} \quad \sqrt{\alpha} \geq \delta/r_B$$

The projection of the group velocity onto the plane orthogonal to \mathbf{B} can be approximately written near the singular point as

$$v_{\perp} \simeq v_{gr}^0 \sqrt{K_1^2 (\Delta p_x)^2 + K_2^2 (\Delta p_y)^2},$$

where v_{gr}^0 is the group velocity at the singular point. Thus, on the trajectory we can, using (VI.2), write near the singular point

$$v_{\perp} \simeq v_{gr}^0 \sqrt{(K_1 K_2 + K_2^2) (\Delta p_y)^2 + \alpha K_1 |\xi_{\mathbf{p}}|},$$

and the velocity of passing the trajectory in \mathbf{p} -space is respectively

$$\frac{eB}{c} v_{gr}^0 \sqrt{(K_1 K_2 + K_2^2) (\Delta p_y)^2 + \alpha K_1 |\xi_{\mathbf{p}}|}$$

The trajectory length element in the \mathbf{p} -space can be written in the form

$$\begin{aligned} dl_{\mathbf{p}} &= \sqrt{(dp_x)^2 + (dp_y)^2} = \\ &= dp_y \sqrt{\left(\frac{K_2 \Delta p_x}{K_1 \Delta p_x}\right)^2 + 1} = \\ &= dp_y \frac{\sqrt{(K_1 K_2 + K_2^2) (\Delta p_y)^2 + \alpha K_1 |\xi_{\mathbf{p}}|}}{\sqrt{K_1 K_2 (\Delta p_y)^2 + \alpha K_1 |\xi_{\mathbf{p}}|}} \end{aligned}$$

Thus, the time of passing the section $dl_{\mathbf{p}}$ is equal to

$$dt = \frac{c}{eB v_{gr}^0} \frac{dp_y}{\sqrt{K_1 K_2 (\Delta p_y)^2 + \alpha K_1 |\xi_{\mathbf{p}}|}}$$

The total time of increasing of the circulation period along a special extremal trajectory due to the presence of the ‘‘deceleration section’’ can be (somewhat formally) estimated as

$$\begin{aligned} T_1 &\simeq \frac{c}{eB v_{gr}^0} \int_{\Delta p_y = -p_F}^{\Delta p_y = p_F} \frac{dp_y}{\sqrt{K_1 K_2 (\Delta p_y)^2 + \alpha K_1 |\xi_{\mathbf{p}}|}} = \\ &= \frac{c}{eB v_{gr}^0} \frac{1}{\sqrt{K_1 K_2}} \ln \left(\frac{\sqrt{\alpha |\xi_{\mathbf{p}}| + K_2 p_F^2} + \sqrt{K_2} p_F}{\sqrt{\alpha |\xi_{\mathbf{p}}| + K_2 p_F^2} - \sqrt{K_2} p_F} \right) \end{aligned}$$

In general, we have

$$\begin{aligned} &\frac{c}{eB v_{gr}^0} \int_{\Delta p_y = -P}^{\Delta p_y = P} \frac{dp_y}{\sqrt{K_1 K_2 (\Delta p_y)^2 + \alpha K_1 |\xi_{\mathbf{p}}|}} = \quad (\text{VI.3}) \\ &= \frac{c}{eB v_{gr}^0} \frac{1}{\sqrt{K_1 K_2}} \ln \left(\frac{\sqrt{\alpha |\xi_{\mathbf{p}}| + K_2 P^2} + \sqrt{K_2} P}{\sqrt{\alpha |\xi_{\mathbf{p}}| + K_2 P^2} - \sqrt{K_2} P} \right) \end{aligned}$$

In the limit

$$\frac{K_2 p_F^2}{\alpha |\xi_{\mathbf{p}}|} \gg 1$$

or just

$$\alpha \ll 1$$

we can write

$$T_1 \simeq \frac{c}{eB v_{gr}^0} \frac{1}{\sqrt{K_1 K_2}} \ln \frac{4K_2 p_F^2}{\alpha |\xi_{\mathbf{p}}|}$$

It is easy to see that in the centrally symmetric case we are considering, the time T_1 should actually be doubled due to the presence of two identical ‘‘deceleration sections’’ on the extremal trajectory. Here we can also see that for any definition of T_1 , the total period of circulation along the trajectory under consideration grows linearly in $\ln 1/\alpha$ with decreasing α with the coefficient $2c/eB v_{gr}^0 \sqrt{K_1 K_2}$. This circumstance can be used, in particular, to determine the value of $v_{gr} \sqrt{K_1 K_2}$ at the corresponding limit singular points of (I.1), i.e. on the curves $\hat{\gamma}_{1,2}$.

For the principle curvatures here, as above, we can use the estimates $K_1 \simeq K_2 \simeq p_F^{-1}$ and write the estimate

$$T_1 \simeq \frac{c p_F}{eB v_{gr}^0} \ln \frac{4p_F}{\alpha |\xi_{\mathbf{p}}|}$$

As for the value of $|\xi_{\mathbf{p}}|$, it can be of the order of p_F (for the simplest trajectories) or several times larger (or

an order of magnitude). For a rough estimate of the time T_1 , we can use the relation

$$T_1 \simeq \frac{r_B}{v_F} \ln \frac{1}{\alpha}$$

For very small values of α the doubled time T_1 can be considered approximately equal to the period of circulation along a special extremal trajectory (if it exceeds the time $T_0 \simeq 2\pi r_B/v_F$ or is comparable with it).

To estimate the time spent by electrons in the skin layer, note that the corresponding section of the trajectory in \mathbf{p} -space corresponds to the values of Δp_x , satisfying the relation

$$\sqrt{\frac{\alpha |\xi_{\mathbf{p}}|}{K_1}} \leq \Delta p_x \leq \sqrt{\frac{\alpha |\xi_{\mathbf{p}}|}{K_1}} + \frac{\delta}{r_B} p_F$$

Substituting the second value in the equation (VI.2), we get the relation for the boundary values of Δp_y

$$K_2 (\Delta p_y)^2 = 2\sqrt{K_1 \alpha |\xi_{\mathbf{p}}|} \frac{\delta}{r_B} p_F + K_1 \frac{\delta^2}{r_B^2} p_F^2$$

Substituting the found values into the integral (VI.3), we will thus find the time T_2 spent by an electron in the skin layer. Here, however, we will not present these calculations in a general form, but consider only two limiting cases:

$$\sqrt{\frac{\alpha |\xi_{\mathbf{p}}|}{K_1}} \ll \frac{\delta}{r_B} p_F \quad \text{and} \quad \sqrt{\frac{\alpha |\xi_{\mathbf{p}}|}{K_1}} \gg \frac{\delta}{r_B} p_F$$

or, in a rough approximation:

$$\sqrt{\alpha} \ll \delta/r_B \quad \text{and} \quad \sqrt{\alpha} \gg \delta/r_B$$

In the first case, we can write

$$\Delta p_y = \pm \sqrt{\frac{K_1}{K_2}} \frac{\delta}{r_B} p_F$$

and write the corresponding value for T_2 in the form

$$T_2 \simeq \frac{c}{eBv_{gr}^0} \frac{1}{\sqrt{K_1 K_2}} \times \ln \left(\frac{\sqrt{\alpha |\xi_{\mathbf{p}}|} + K_1 \delta^2 p_F^2 / r_B^2 + \sqrt{K_1} \delta p_F / r_B}{\sqrt{\alpha |\xi_{\mathbf{p}}|} + K_1 \delta^2 p_F^2 / r_B^2 - \sqrt{K_1} \delta p_F / r_B} \right)$$

Using the same assumption, we can now write also

$$T_2 \simeq \frac{c}{eBv_{gr}^0} \frac{1}{\sqrt{K_1 K_2}} \ln \frac{4K_1 p_F^2 \delta^2}{\alpha |\xi_{\mathbf{p}}| r_B^2}$$

We can see that the ratio of times T_2/T_1 in this case is equal to

$$\left(\ln \frac{4K_1 p_F^2}{\alpha |\xi_{\mathbf{p}}|} - \ln \frac{r_B^2}{\delta^2} \right) / \ln \frac{4K_1 p_F^2}{\alpha |\xi_{\mathbf{p}}|}$$

and under our assumption is close to unity. It can be noted that the same ratio in the case of getting of a "normal part" of a trajectory into the skin layer is of the order of $\sqrt{\delta/r_B}$ and represents a small value. As a consequence of this, the amplitude of oscillations in the absorption of the incident radiation can be noticeably higher here in comparison with the "ordinary" case. It should also be noted that the condition

$$\frac{\alpha |\xi_{\mathbf{p}}|}{4K_1 p_F^2} \ll \frac{\delta^2}{r_B^2}$$

is actually quite strong and can be observed only in sufficiently strong magnetic fields and at very small angles α . Thus, using again rough estimates for K_1 and $|\xi_{\mathbf{p}}|$, this condition can be written as $\alpha \ll \delta^2/r_B^2$. We can see that this condition in reality implies the relations $\delta/r_B \simeq 10^{-1}$ (strong magnetic fields $B \simeq 10 Tl$) and $\alpha \leq 10^{-3}$.

As for the opposite limit

$$\sqrt{\frac{\alpha |\xi_{\mathbf{p}}|}{K_1}} \gg \frac{\delta}{r_B} p_F$$

(but, as before, $\alpha \ll 1$), it is, on the contrary, observed at not very strong magnetic fields. Here, as above, we can write the relation for rough estimation

$$\sqrt{\alpha} \gg \delta/r_B$$

For example, for the values of B of order of $1 Tl$ we can take $\delta/r_B \simeq 10^{-2}$ and the required condition is satisfied for $\alpha \geq 10^{-3}$. For $B \simeq 10 Tl$ we have the relation $\delta/r_B \simeq 10^{-1}$ and then we should assume $\alpha \gg 10^{-2}$.

Let us also use a rough estimate for the values Δp_y , bounding the region corresponding to the stay of the electron in the skin layer

$$\Delta p_y = p_F \sqrt{\sqrt{\alpha} \delta / r_B}$$

After substituting these values into the integration limits in (VI.3), we get

$$T_2 \simeq \frac{c}{eBv_{gr}^0} \frac{1}{\sqrt{K_1 K_2}} \times \ln \left(\frac{\sqrt{1 + \delta/(r_B \sqrt{\alpha})} + \sqrt{\delta/(r_B \sqrt{\alpha})}}{\sqrt{1 + \delta/(r_B \sqrt{\alpha})} - \sqrt{\delta/(r_B \sqrt{\alpha})}} \right) \simeq$$

$$\simeq \frac{2c}{eBv_{gr}^0} \frac{1}{\sqrt{K_1 K_2}} \sqrt{\delta/(r_B \sqrt{\alpha})} \simeq \frac{2r_B}{v_F} \sqrt{\delta/(r_B \sqrt{\alpha})}$$

Note that the time ratio T_2/T here is formally larger than $\sqrt{\delta/r_B}$ for $\alpha \ll 1$. However, substituting the above real values of α for this limit, we can see in fact that the value of $1/\sqrt[4]{\alpha}$ is not very large. It can be seen, therefore, that in the case under consideration, this ratio

is of the order of the same ratio for the case when an “ordinary” section of an extremal trajectory enters the skin layer. In fact, this is not a contradiction, because, although the section under consideration is a “deceleration section”, the curvature of the trajectory on it is much larger than the curvature on “ordinary” sections. Thus, in the limit we are considering, we should expect approximately the same amplitude of oscillations in the absorption of the incident radiation compared with the cyclotron resonance in the “standard” situation.

In general, we can see that when the “deceleration section” hits the skin layer, the behavior of the amplitude of oscillations of absorption of the incident radiation differs noticeably from its behavior in the “usual” situation. In particular, the amplitude of the absorption oscillations can be of the order of the same amplitude in the “standard” case when the direction of \mathbf{B} is not too close to the boundary of the reconstruction of the structure of system (I.1). With more precise approximation of the direction of \mathbf{B} to the boundary of reconstruction of the structure of (I.1), the amplitude of the oscillations increases and at very small α and in sufficiently strong magnetic fields can noticeably exceed the amplitude of such oscillations in the “standard” case.

It can also be seen that, for the same reasons, the intensity of the current layers, corresponding to the “deceleration sections”, inside the sample (when the “normal” section of the trajectory enters the skin layer (Fig. 48)) should not be very large for not very precise approach of the direction of \mathbf{B} to the boundary of the reconstruction of the structure of system (I.1) and should increase markedly with a more precise approach of the direction of \mathbf{B} to this boundary. In particular, their intensity should be comparable with the intensity of the current layers corresponding to the sections at which the group velocity is parallel to the sample boundary, in the limit $\sqrt{\alpha} \gg \delta/r_B$, and can noticeably exceed it in the limit $\sqrt{\alpha} \ll \delta/r_B$.

Here, however, we need to make a few more remarks about the amplitude of oscillations at a very close approximation of the direction of \mathbf{B} to a boundary of the reconstruction of the structure of system (I.1).

First, as we said above, in this approximation the height of the corresponding cylinder of closed trajectories becomes very small. Due to this circumstance, the measure of trajectories near the special extremal trajectory, contributing to the corresponding oscillation term, can also decrease. This effect, as we see, is opposite to the effect described above, so that, possibly, as a result, the amplitude of the corresponding oscillation term may not significantly exceed its amplitude in the “standard” situation. The exact picture of the behavior of the corresponding oscillation amplitude depends, in fact, on the features of the geometry of the Fermi surface near the special extremal trajectory and on the experimental conditions.

Another distinctive feature in observing the cyclotron resonance when a “deceleration section” enters the skin

layer is that, at very small α , the decreasing of the amplitude of the observed oscillations with increasing number $n = T\Omega/2\pi = T\nu$ here should be much faster compared to the case of “ordinary” extremal closed trajectories. The reason for this is that, due to the long time spent by electron in the skin layer, n cannot be too large, otherwise the field \mathbf{E}_w can become oscillating already at the time of the electron’s presence in the skin layer, which significantly reduces the efficiency of energy accumulation during this time. As we saw above, in the limit of the extreme proximity of the singular points of system (I.1) to the trajectories under consideration, the time spent by the electron in the skin layer can become comparable with the period T of circulation along the entire trajectory. In this situation, only a few peaks of oscillations of rapidly decreasing amplitude are likely to have a relatively large value. (For comparison, it can be noted here that for cyclotron resonance on ordinary trajectories, the number of observed peaks in similar oscillating terms can reach several tens). A sharp decrease in the number of observed peaks in the absorption amplitude can also serve as an indication of the approach of the direction of \mathbf{B} to the boundary of the reconstruction of the topological structure of system (I.1).

Finally, let us make one more remark here. According to the general idea of this paper, it is obvious that we would like to study oscillation phenomena as close as possible to the “net” of directions of \mathbf{B} , corresponding to the reconstructions of the structure of (I.1). As for the restrictions on the approximation of the direction of \mathbf{B} to the curve of a reconstruction of the structure of (I.1) while maintaining the observation conditions for oscillation phenomena on special extremal trajectories, we can immediately distinguish two such restrictions. The first can be attributed to an increase in the period T of circulation along extremal trajectories, while the observation of the oscillation phenomena requires the condition $\tau/T \gg 1$. As we noted above, this condition is not really too restrictive, since the growth of T is rather slow (logarithmic) when approaching the boundary of a reconstruction.

The second limitation can be attributed to the phenomenon of magnetic breakdown between two close sections of trajectories close to a singular one, as the direction of \mathbf{B} approaches the boundary of the reconstruction of system (I.1) (Fig. 56).

Here we will also not consider in detail the theory of magnetic breakdown, which leads to many different effects for various trajectories of the system (I.1) (see e.g. [1–3, 52–56]). In our case, it is obvious that the “simple” picture of oscillation phenomena that we assume on special extremal trajectories should arise in a situation where the probability of magnetic breakdown is close to zero. In our situation we are dealing with the intraband magnetic breakdown, the probability of which becomes significant when the height of the classical potential barrier between close sections of the trajectory approaches the value $\mu_B B$. The height of the classical potential bar-

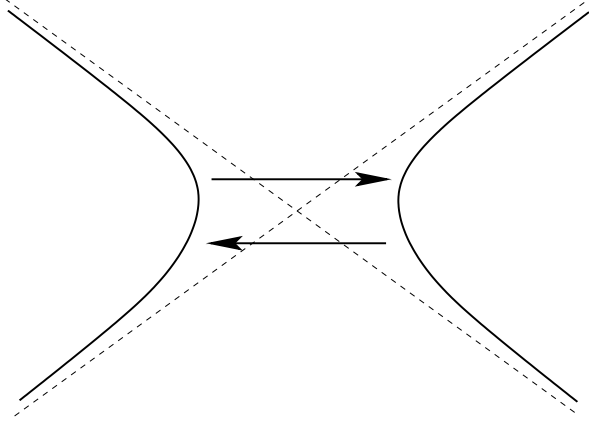


FIG. 56: The phenomenon of magnetic breakdown between two “deceleration sections” on trajectories approaching singular ones.

rier is directly related to the angle α and, as it is not difficult to see, can be estimated as

$$\Delta\epsilon \simeq v_{gr}^0 \frac{\alpha |\xi_{\mathbf{p}}|}{2} \simeq v_F \frac{\alpha |\xi_{\mathbf{p}}|}{2} \simeq \frac{\alpha \epsilon_F |\xi_{\mathbf{p}}|}{2 p_F},$$

such that

$$\frac{\Delta\epsilon}{\mu_B B} \simeq \frac{\epsilon_F}{\mu_B B} \frac{\alpha |\xi_{\mathbf{p}}|}{2 p_F}$$

In the roughest approximation, we can actually write

$$\frac{\Delta\epsilon}{\mu_B B} \simeq \frac{\epsilon_F}{\mu_B B} \alpha$$

Taking the values $\mu_B \simeq 5.8 \cdot 10^{-5} eV/Tl$ and $\epsilon_F \simeq 5 eV$, we can see that

$$\frac{\Delta\epsilon}{\mu_B B} \simeq 10^5 \alpha \quad \text{at} \quad B \simeq 1 Tl$$

and

$$\frac{\Delta\epsilon}{\mu_B B} \simeq 10^4 \alpha \quad \text{at} \quad B \simeq 10 Tl$$

Thus, we can see that the “simple” picture of oscillation phenomena (classical or quantum) is limited by the values $\alpha \geq 10^{-5}$ at $B \simeq 1 Tl$ and $\alpha \geq 10^{-4}$ at $B \simeq 10 Tl$. In particular, one may ask about the possibility of observing such a picture in the above limit

$$\sqrt{\frac{\alpha |\xi_{\mathbf{p}}|}{K_1}} \ll \frac{\delta}{r_B} p_F \quad \text{or} \quad \sqrt{\alpha} \ll \delta/r_B$$

in the case of the cyclotron resonance.

Going back to the previous estimates $\delta/r_B \simeq 10^{-1}$ ($B \simeq 10 Tl$) and $\alpha \leq 10^{-3}$ for such a situation, it can be seen that this limit, in fact, may have certain restrictions due to the magnetic breakdown.

VII. CONCLUSIONS

The paper considers issues related to reconstructions of the topological structure of a dynamical system that describes the semiclassical motion of electrons on complex Fermi surfaces in the presence of an external magnetic field. In particular, the paper lists all types of elementary reconstructions of the structure of this system and describes special closed extremal trajectories, the appearance of which always accompanies such reconstructions. It is shown that the oscillation phenomena corresponding to the appearance of such trajectories may have certain special features. The study of oscillation phenomena associated with special extremal trajectories can be a useful tool for the study of electronic spectra in metals.

The study was carried out at the expense of a grant from the Russian Science Foundation (project № 18-11-00316).

-
- [1] C. Kittel., Quantum Theory of Solids., Wiley, 1963.
 - [2] I.M. Lifshitz, M.Ya. Azbel, M.I. Kaganov., Electron Theory of Metals. Moscow, Nauka, 1971. Translated: New York: Consultants Bureau, 1973.
 - [3] A.A. Abrikosov., Fundamentals of the Theory of Metals., Elsevier Science & Technology, Oxford, United Kingdom, 1988.
 - [4] I.M.Lifshitz, M.Ya.Azbel, M.I.Kaganov. The Theory of Galvanomagnetic Effects in Metals., *Sov. Phys. JETP* 4:1, 41-53 (1957).
 - [5] I.M. Lifshitz, V.G. Peschansky., Galvanomagnetic char-

- acteristics of metals with open Fermi surfaces., *Sov. Phys. JETP* 8:5, 875-883 (1959).
- [6] I.M. Lifshitz, V.G. Peschansky., Galvanomagnetic characteristics of metals with open Fermi surfaces. II., *Sov. Phys. JETP* 11:1, 131-141 (1960).
- [7] I.M. Lifshitz, M.I. Kaganov., Some problems of the electron theory of metals I. Classical and quantum mechanics of electrons in metals., *Sov. Phys. Usp.* 2:6 (1960), 831-835.
- [8] I.M. Lifshitz, M.I. Kaganov., Some problems of the electron theory of metals II. Statistical mechanics and ther-

- modynamics of electrons in metals., *Sov. Phys. Usp.* **5:6** (1963), 878-907.
- [9] I.M. Lifshitz, M.I. Kaganov., Some problems of the electron theory of metals III. Kinetic properties of electrons in metals., *Sov. Phys. Usp.* **8:6** (1966), 805-851.
- [10] Conductivity electrons., Red. M.I. Kaganov, V.S. Edelman., Moscow, Nauka, 1985 (in Russian).
- [11] M.I. Kaganov, V.G. Peschansky., Galvano-magnetic phenomena today and forty years ago., *Physics Reports* **372** (2002), 445-487.
- [12] S.P. Novikov., The Hamiltonian formalism and a many-valued analogue of Morse theory., *Russian Math. Surveys* **37** (5) (1982), 1-56.
- [13] A.V. Zorich., A problem of Novikov on the semiclassical motion of an electron in a uniform almost rational magnetic field., *Russian Math. Surveys* **39** (5) (1984), 287-288.
- [14] I.A. Dynnikov., Proof of S.P. Novikov's conjecture for the case of small perturbations of rational magnetic fields., *Russian Math. Surveys* **47** (3) (1992), 172-173.
- [15] S.P. Tsarev. Private communication. (1992-93).
- [16] I.A. Dynnikov., Proof of S.P. Novikov's conjecture on the semiclassical motion of an electron., *Math. Notes* **53:5** (1993), 495-501.
- [17] A.V. Zorich., Proc. "Geometric Study of Foliations", (Tokyo, November 1993) / ed. T.Mizutani et al. Singapore: World Scientific, 479-498 (1994).
- [18] I.A. Dynnikov., Surfaces in 3-torus: geometry of plane sections., Proc. of ECM2, BuDA, 1996.
- [19] I.A. Dynnikov., Semiclassical motion of the electron. A proof of the Novikov conjecture in general position and counterexamples., Solitons, geometry, and topology: on the crossroad, Amer. Math. Soc. Transl. Ser. 2, 179, Amer. Math. Soc., Providence, RI, 1997, 45-73.
- [20] I.A. Dynnikov., The geometry of stability regions in Novikov's problem on the semiclassical motion of an electron., *Russian Math. Surveys* **54:1** (1999), 21-59.
- [21] R. De Leo., First-principles generation of stereographic maps for high-field magnetoresistance in normal metals: An application to Au and Ag., *Physica B: Condensed Matter* **362** (1-4) (2005), 62-75.
- [22] S.P. Novikov, A.Y. Maltsev., Topological quantum characteristics observed in the investigation of the conductivity in normal metals., *JETP Letters* **63** (10) (1996), 855-860.
- [23] S.P. Novikov, A.Y. Maltsev., Topological phenomena in normal metals., *Physics-Uspokhi* **41:3** (1998), 231-239.
- [24] A.Ya. Maltsev, S.P. Novikov., Quasiperiodic functions and Dynamical Systems in Quantum Solid State Physics., *Bulletin of Braz. Math. Society, New Series* **34:1** (2003), 171-210.
- [25] A.Ya. Maltsev, S.P. Novikov., Dynamical Systems, Topology and Conductivity in Normal Metals in strong magnetic fields., *Journal of Statistical Physics* **115**:(1-2) (2004), 31-46.
- [26] A.V. Zorich., Finite Gauss measure on the space of interval exchange transformations. Lyapunov exponents., *Annales de l'Institut Fourier* **46:2**, (1996), 325-370.
- [27] Anton Zorich., On hyperplane sections of periodic surfaces., Solitons, Geometry, and Topology: On the Crossroad, V. M. Buchstaber and S. P. Novikov (eds.), Translations of the AMS, Ser. 2, vol. **179**, AMS, Providence, RI (1997), 173-189.
- [28] Anton Zorich., How do the leaves of closed 1-form wind around a surface., "Pseudoperiodic Topology", V.I. Arnold, M. Kontsevich, A. Zorich (eds.), Translations of the AMS, Ser. 2, vol. 197, AMS, Providence, RI, 1999, 135-178.
- [29] R. De Leo., On the semiclassical motion of an electron., *Russian Math. Surveys* **55:1** (2000), 166-168.
- [30] R. De Leo., Characterization of the set of "ergodic directions" in Novikov's problem of quasi-electron orbits in normal metals., *Russian Math. Surveys* **58:5** (2003), 1042-1043.
- [31] Anton Zorich., Flat surfaces., in collect. "Frontiers in Number Theory, Physics and Geometry. Vol. 1: On random matrices, zeta functions and dynamical systems"; Ecole de physique des Houches, France, March 9-21 2003, P. Cartier; B. Julia; P. Moussa; P. Vanhove (Editors), Springer-Verlag, Berlin, 2006, 439-586.
- [32] R. De Leo, I.A. Dynnikov., An example of a fractal set of plane directions having chaotic intersections with a fixed 3-periodic surface.,
- [33] A. Skripchenko., Symmetric interval identification systems of order three., *Discrete Contin. Dyn. Sys.* **32:2** (2012), 643-656.
- [34] A. Skripchenko., On connectedness of chaotic sections of some 3-periodic surfaces., *Ann. Glob. Anal. Geom.* **43** (2013), 253-271.
- [35] I. Dynnikov, A. Skripchenko., On typical leaves of a measured foliated 2-complex of thin type., Topology, Geometry, Integrable Systems, and Mathematical Physics: Novikov's Seminar 2012-2014, Advances in the Mathematical Sciences., Amer. Math. Soc. Transl. Ser. 2, 234, eds. V.M. Buchstaber, B.A. Dubrovin, I.M. Krichever, Amer. Math. Soc., Providence, RI, 2014, 173-200, arXiv: 1309.4884
- [36] I. Dynnikov, A. Skripchenko., Symmetric band complexes of thin type and chaotic sections which are not actually chaotic., *Trans. Moscow Math. Soc.*, Vol. 76, no. 2, 2015, 287-308.
- [37] A. Avila, P. Hubert, A. Skripchenko., Diffusion for chaotic plane sections of 3-periodic surfaces., *Inventiones mathematicae*, October 2016, Volume 206, Issue 1, pp 109-146.
- [38] A. Avila, P. Hubert, A. Skripchenko., On the Hausdorff dimension of the Rauzy gasket., *Bulletin de la societe mathematique de France*, 2016, **144** (3), pp. 539 - 568.
- [39] Roberto De Leo., A survey on quasiperiodic topology., Advanced Mathematical Methods in Biosciences & Applications, Springer, Eds. F. Berezovskaya and B. Toni, (2018)., arXiv:1711.01716
- [40] A.Ya. Maltsev, S.P. Novikov., Topological integrability, classical and quantum chaos, and the theory of dynamical systems in the physics of condensed matter., *Russian Mathematical Surveys* **74(1)** (2019), 141-173
- [41] Rodolfo Gutierrez-Romo, Carlos Matheus., Lower bounds on the dimension of the Rauzy gasket., arXiv:1902.04516 [math.DS]
- [42] S.P. Novikov, R. De Leo, I.A. Dynnikov, A.Ya. Maltsev., Theory of Dynamical Systems and Transport Phenomena in Normal Metals., *Journal of Experimental and Theoretical Physics* **129:4** (2019), 710-721
- [43] A.Ya. Maltsev., The complexity classes of angular diagrams of the metal conductivity in strong magnetic fields., *Journal of Experimental and Theoretical Physics* **129:1** (2019), 116-138
- [44] A.Ya. Maltsev., On the Analytical Properties of the

- Magneto-Conductivity in the Case of Presence of Stable Open Electron Trajectories on a Complex Fermi Surface., *Journal of Experimental and Theoretical Physics* **124** (5) (2017), 805-831.
- [45] A.Ya. Maltsev., Oscillation phenomena and experimental determination of exact mathematical Stability Zones for magneto-conductivity in metals having complicated Fermi surfaces., *Journal of Experimental and Theoretical Physics* **125**
- [46] A.Ya. Maltsev., The second boundaries of Stability Zones and the angular diagrams of conductivity for metals having complicated Fermi surfaces., *Journal of Experimental and Theoretical Physics* **127**:6 (2018), 1087-1111., arXiv:1804.10762
- [47] E.A. Kaner, Cyclotronic resonance in films, Dokl. Akad. Nauk SSSR, **119**:3 (1958), 471-474
- [48] V.F. Gantmakher, Dimensional Effect in a Metal in Multiples of a Certain Magnetic Field., *Journal of Experimental and Theoretical Physics* **16**:1 (1963), 247-249
- [49] M. Orlita, P. Neugebauer, C. Faugeras, A.-L. Barra, M. Potemski, F.M.D. Pellegrino, and D.M. Basko., Cyclotron Motion in the Vicinity of a Lifshitz Transition in Graphite., *Phys. Rev. Lett.* **108**, 017602, arXiv:1109.5014
- [50] M.Ia. Azbel, E.A. Kaner., The Theory of Cyclotron Resonance in Metals., *Journal of Experimental and Theoretical Physics* **3**:5 (1956), 772-774
- [51] M.Ia. Azbel, E.A. Kaner., Theory of Cyclotron Resonance in Metals., *Journal of Experimental and Theoretical Physics* **5**:4 (1957), 730-744
- [52] G.E. Zil'berman, Behavior of an Electron in a Periodic Electric and a Uniform Magnetic Field., *Journal of Experimental and Theoretical Physics* **5**:2 (1957), 208-215
- [53] G.E. Zil'berman, Electron in a Periodic Electric and Homogenous Magnetic Field, II., *Journal of Experimental and Theoretical Physics* **6**:2 (1958), 299-306
- [54] G.E. Zil'berman, Motion of Electron along Self-Intersecting Trajectories., *Journal of Experimental and Theoretical Physics* **7**:3 (1958), 513-514
- [55] M.Ia. Azbel, Quasiclassical Quantization in the Neighborhood of Singular Classical Trajectories., *Journal of Experimental and Theoretical Physics* **12**:5 (1961), 891-897
- [56] A. Alexandradinata and Leonid Glazman., Semiclassical theory of Landau levels and magnetic breakdown in topological metals., arXiv: 1710.04215